

## RESEARCH ARTICLE

10.1002/2015JB012778

## Key Points:

- The central Jiangnan Orogen experienced four stages of deformation in the Phanerozoic
- Early Paleozoic NW-SE contraction led to combined dextral and NW directed thrust shearing
- Mesozoic episodic contraction and extension result from plate subduction/collision along boundaries

## Supporting Information:

- Supporting Information S1

## Correspondence to:

S. Dong,  
swdong8888@126.com  
swdong@cags.ac.cn

## Citation:

Li, J., S. Dong, Y. Zhang, G. Zhao, S. T. Johnston, J. Cui, and Y. Xin (2016), New insights into Phanerozoic tectonics of south China: Part 1, polyphase deformation in the Jiuling and Lianyunshan domains of the central Jiangnan Orogen, *J. Geophys. Res. Solid Earth*, 121, 3048–3080, doi:10.1002/2015JB012778.

Received 27 DEC 2015

Accepted 29 MAR 2016

Accepted article online 5 APR 2016

Published online 21 APR 2016

## New insights into Phanerozoic tectonics of south China: Part 1, polyphase deformation in the Jiuling and Lianyunshan domains of the central Jiangnan Orogen

Jianhua Li<sup>1,2</sup>, Shuwen Dong<sup>3</sup>, Yueqiao Zhang<sup>3</sup>, Guochun Zhao<sup>1</sup>, Stephen T. Johnston<sup>4</sup>, Jianjun Cui<sup>2</sup>, and Yujia Xin<sup>2</sup>

<sup>1</sup>Department of Earth Sciences, James Lee Science Building, The University of Hong Kong, Hong Kong, China, <sup>2</sup>Institute of Geomechanics, Chinese Academy of Geological Sciences, Beijing, China, <sup>3</sup>School of Earth Sciences and Engineering, Nanjing University, Nanjing, China, <sup>4</sup>Earth and Atmospheric Sciences, Earth Sciences Building, University of Alberta, Edmonton, Alberta, Canada

**Abstract** The central Jiangnan Orogen, genetically formed by the Proterozoic Yangtze-Cathaysia collision, presents as a composite structural feature in the Phanerozoic with multiple ductile and brittle fabrics whose geometries, kinematics, and ages are crucial to decipher the tectonic evolution of south China. New structural observations coupled with thermochronological and geochronological studies of these fabrics document four main stages of deformation. The earliest stage in early Paleozoic time (460–420 Ma) corresponds to combined E-trending dextral and northwest directed thrust shearing that was variably partitioned in anastomosing high-strain zones under greenschist-facies conditions (~400–500°C), related to the continued Yangtze-Cathaysia convergence externally driven by the suturing of south China with Australia. This event was heterogeneously overprinted by the second stage characterized by ~E-oriented folding in middle Triassic time, geodynamically resulting from the continental collision of south China with Indochina and North China. The third stage was locally developed by northwest and southeast vergent thrusts that truncated ~E-oriented folds in the Late Jurassic, due to northwestward subduction of the Paleo-Pacific plate. The latest stage involved normal faulting and tectonic unroofing in Cretaceous time, which resulted in basin opening and reset footwall <sup>40</sup>Ar/<sup>39</sup>Ar ages in proximity to the Hengshan detachment fault, associated with roll-back of the subducting Paleo-Pacific plate.

### 1. Introduction

South China is one of the most important continental terranes that form present-day Southeast Asia [e.g., Carter *et al.*, 2001; Faure *et al.*, 2009]. It is separated from North China by the Qinling-Dabie orogen and consists of the Yangtze and Cathaysia Blocks (Figure 1). These two crustal blocks are traditionally interpreted to have amalgamated during a Proterozoic collision [e.g., Chen *et al.*, 1991; Shu *et al.*, 1994; Shu and Charvet, 1996; Charvet *et al.*, 1996; Li *et al.*, 2002, 2007; X. L. Wang *et al.*, 2007; Dong *et al.*, 2015]. The Phanerozoic tectonic evolution of south China is characterized by three discrete orogenic cycles including early Paleozoic, Triassic, and Jurassic-Cretaceous orogenies, respectively [e.g., Lin *et al.*, 2008; Wang *et al.*, 2013a; G. W. Zhang *et al.*, 2013].

The early Paleozoic orogeny, termed the Wuyi-yunkai/Kwangian orogeny [Shu *et al.*, 2008a; Faure *et al.*, 2009; Charvet *et al.*, 2010; Z. X. Li *et al.*, 2010; Wang *et al.*, 2013a], was recognized due to conspicuous development of a regional Middle or Late Devonian unconformity; a hiatus of Silurian sedimentation; early Paleozoic greenschist to amphibolite facies metamorphism, ductile shearing, folding, and crustal melting; and voluminous Silurian magmatism [e.g., Grabau, 1924; Ting, 1929; Huang *et al.*, 1980; Lin *et al.*, 2008; Charvet *et al.*, 2010; Shu *et al.*, 2008a, 2014, 2015; Wang *et al.*, 2011, 2012; Charvet, 2013; Li *et al.*, New insights into Phanerozoic tectonics of South China: Part 2, Early Paleozoic sinistral and Triassic dextral transpression in the north Cathaysia, under review, 2016]. Although intense research has been conducted, many controversies regarding the nature and tectonic environment of the orogeny remain. Some authors emphasize the existence of a Neoproterozoic-Paleozoic ocean between the Yangtze and Cathaysia Blocks and invoked an early Paleozoic arc-continent collision involving northwestward subduction of their intervening oceanic lithosphere, ocean closure, and arc-continent collision to explain the orogenic event [e.g., Guo *et al.*, 1989; Chen *et al.*, 2006]. However, the validity of this model has been questioned by others due to the absence of early Paleozoic ophiolite suites, deep-sea sedimentary rocks, and arc magmatism [e.g., Shu *et al.*, 2008b, 2014; Wang *et al.*, 2011]. An alternative model, in which the

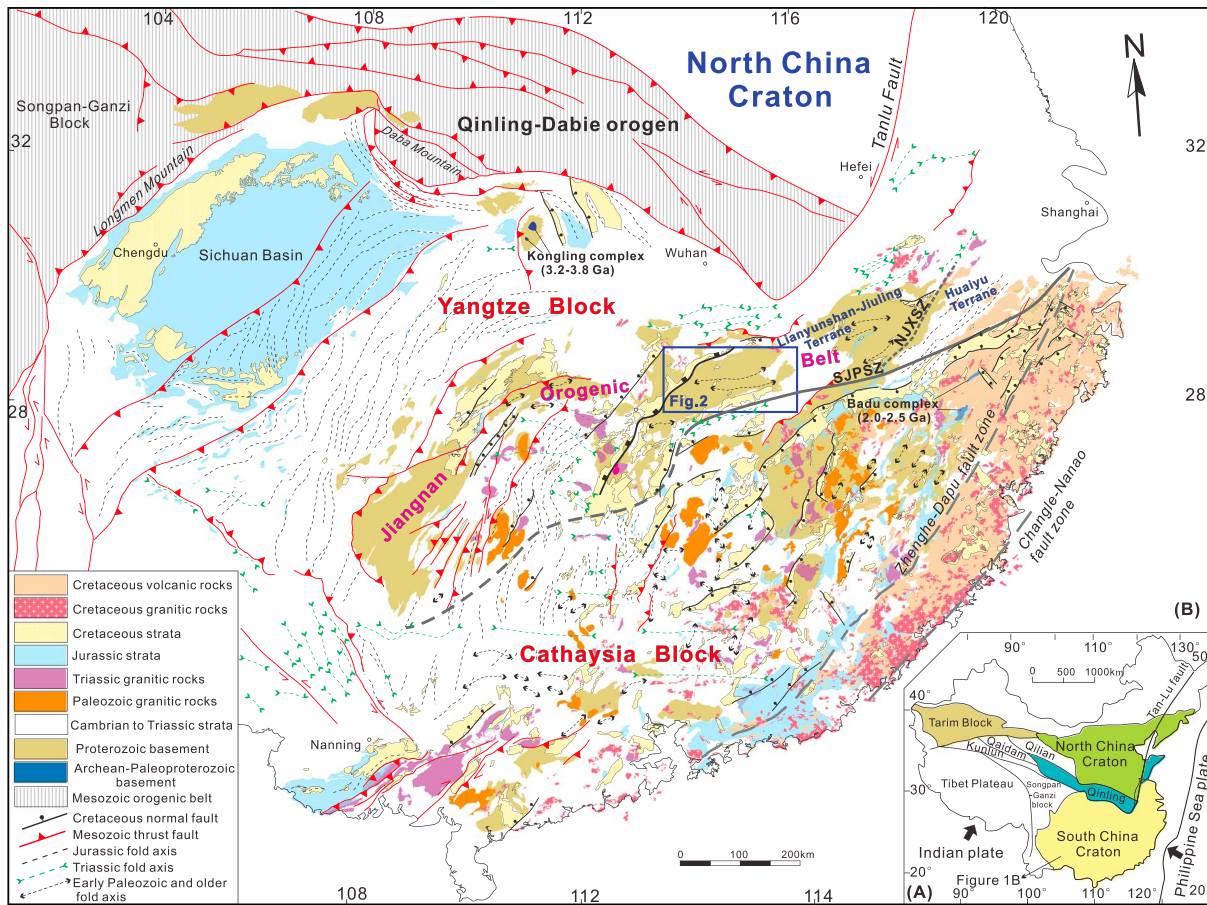


**Figure 1.** (a) Sketch map showing the location of south China (modified after *Li et al.* [2015a]). (b) Simplified geological map of south China delineating the distributions of major Phanerozoic structures and igneous rocks. SJPSZ, Shaoxing-Jiangshan-Pingxiang suture zone. NJXSZ, Northeastern Jiangxi suture zone.

Yangtze and Cathaysia Blocks are interpreted to have been joined together since the Neoproterozoic, highlights that this orogeny was an intraplate event [e.g., *Charvet et al.*, 1996, 1999; *Chen et al.*, 2000]. Although recent structural and magmatic studies have come to favor the intraplate model for orogeny [*Y. J. Wang et al.*, 2007, 2012; *Faure et al.*, 2009; *Charvet et al.*, 2010; *Z. X. Li et al.*, 2010; *Shu et al.*, 2008a, 2014], the associated intraplate structural framework of south China and the external driving force for the orogeny remain ambiguous.

The Triassic orogeny, also termed the Indosinian orogeny, was originally inferred from a Late Triassic unconformity in Vietnam [e.g., *Deprat*, 1914; *Fromaget*, 1932]. Observations consistent with a Triassic orogeny have been extensively recognized in south China and include Triassic plutonism, ductile shearing, folding, thrusting, and greenschist-facies metamorphism [e.g., *Chen*, 1999; *Wang et al.*, 2005, 2007c; *Lin et al.*, 2008; *Shu et al.*, 2008b, 2009; *Zhang and Cai*, 2009; *Xu et al.*, 2011; *Chu et al.*, 2012]. *Hsu et al.* [1990] first advocated a Mesozoic Yangtze-Cathaysia collision model based on interpretation of the “Banxi ophiolite mélangé” as an early Mesozoic suture during orogeny. Because of the negation of such ophiolite mélangé by subsequent stratigraphic and magmatic studies [e.g., *Wang and Li*, 2003], this hypothesis received little support. The current consensus is that the Indosinian orogeny occurred within an intracontinental geological setting [e.g., *Wang et al.*, 2005; *Li and Li*, 2007; *Shu et al.*, 2015]. Despite this, several competing models have been invoked for describing the mechanics of Triassic intracontinental structures, including those involving flat subduction of the Paleo-Pacific plate [*Li and Li*, 2007], continental collisions with North China and the Indochina Block at block boundaries [e.g., *Zhang and Cai*, 2009; *Faure et al.*, 2014], and a combination of both that vary in space and time due to the interplay between the two dynamic systems [*Wang et al.*, 2013a].

The Jurassic-Cretaceous orogeny began with a Middle-Late Jurassic crustal contraction event that gave rise to a broad (~1300 km wide) NE trending structural belt composed of imbricate thrusts, fault-related folds, multiple detachments, and overthrust nappes [e.g., *Yang and Yu*, 1994; *Ding et al.*, 2007; *Yan et al.*, 2003; *J. H. Li et al.*,

2012]. Subsequent Cretaceous crustal extension generated abundant igneous rocks, extensional basins, and dome structures [Gilder *et al.*, 1991; Zhou *et al.*, 2006; Shu *et al.*, 2009; Kusky *et al.*, 2010; Wang and Shu, 2012; Li *et al.*, 2013]. Geodynamically, the earlier crustal contraction was ascribed to northwestward subduction of the Paleo-Pacific plate [e.g., Zhang *et al.*, 2008], whereas the driving force for later crustal extension has been variously interpreted, including slab rollback of the subducted Paleo-Pacific plate [Zhou and Li, 2000], intracontinental lithospheric extension unrelated to plate subduction [Li, 2000], and slab foundering and delamination of the subducted flat slab [Z. X. Li *et al.*, 2012].

Discriminating among the above models is crucial to the understanding of the Phanerozoic tectonic evolution of south China and its relationship to the evolving dynamics of plate subduction/collision along active boundaries. To evaluate these models, some key questions must be addressed, including the kinematics, geometries, and timing of individual structures, and their tectonic relations in the context of multiphase deformation. This paper represents the first of a two-part series on the Phanerozoic tectonic evolution of south China, by focusing on polyphase deformation in the Jiuling and Lianyunshan domains of the central Jiangnan Orogen. The companion paper will deal with the Paleozoic sinistral and Triassic dextral transpression in the north Cathaysia (Li *et al.*, under review, 2016).

We selected the Jiuling and Lianyunshan domains of the central Jiangnan Orogen for this study because of (1) its central position in the overall architecture of south China (Figure 1) and (2) the exceptionally well-preserved Phanerozoic ductile structures and granitoids that can be directly dated by isotopic methods. Previous studies provide an emerging Phanerozoic picture of punctuated, multiphase deformation events in this orogen, each involving significantly different fabric elements (lineations, cleavages, faults, and folds) [Shu *et al.*, 1991; Chu and Lin, 2014; Xu *et al.*, 2015]. However, distinguishing individual events is a puzzling problem because of poor age constraints, discontinuous exposures, and ambiguous structural relations. This complexity has led to competing interpretations on the overall kinematic evolution through space and times, particularly on the kinematics and timing of individual structural fabrics in the zones with multiphase deformation. For example, the early Paleozoic kinematics of E to NE trending ductile shear zones in the Jiuling domain of the central Jiangnan Orogen were interpreted to be sinistral-lateral by Shu *et al.* [1991], whereas Chu and Lin [2014] favored a dextral-lateral interpretation. Even for the same structural feature, there are many uncertainties about the timing of deformation; for example, the subhorizontal E-W lineations associated with dextral shearing are interpreted to have formed in Middle Silurian time by Xu *et al.* [2015] but are constrained to have formed in Late Devonian time by Chu and Lin [2014]. Therefore, how the Jiangnan Orogen evolved in the Phanerozoic remains controversial. In this study, we document new structural evidence, including ductile shear and brittle fabrics, kinematic criteria, and folds, to establish an improved and more detailed multiphase deformation sequence and estimate the deformation time and temperature conditions for individual structures. Our data provide a framework for understanding the Phanerozoic tectonic evolution of the Jiuling and Lianyunshan domains of the central Jiangnan Orogen and for determining the role of plate subduction and collision in shaping the south China block.

## 2. Geological Overview of the Jiangnan Orogen

### 2.1. Neoproterozoic Basement, Geochronology, and Deformation

The Jiangnan Orogen, as an east-north-east trending orogenic collage in central south China (Figure 1), was developed by protracted oceanic subduction, closure, and collision/amalgamation of island terranes between the Yangtze and Cathaysia Blocks during the Proterozoic [e.g., Guo *et al.*, 1996; Dong *et al.*, 2015; Zhao, 2015; X. L. Wang *et al.*, 2007]. The orogen is bounded to the south by the Shaoxing-Jiangshan-Pingxiang suture zone (SJPSZ) and covered to the north by Phanerozoic sedimentary rocks (Figure 1). Much of this orogen is composed of Precambrian rocks including basement sequences, granites, and mafic rocks (Figure 2). The basement sequences, termed the Shuangxiwu, Xikou, Shuangqiaoshan, Sibao/Fengjingshan/Lengjiayi, and Banxi/Danzhou groups, mainly comprise green-schist facies metamorphosed schist and pelite interbedded with felsic tuff, spilite, and mafic-ultramafic sills and show depositional features of flysch turbidites [e.g., Wang and Li, 2003; X. L. Wang *et al.*, 2007; Yin *et al.*, 2013]. These rock sequences were previously considered to be Mesoproterozoic in age [e.g., Yang *et al.*, 1994]. However, U-Pb zircon age determinations demonstrate that these sequences were formed during the Neoproterozoic, i.e., 980–890 Ma for the Shuangxiwu Group [Zhang *et al.*, 1990; Li *et al.*, 2009], 880–820 Ma for the

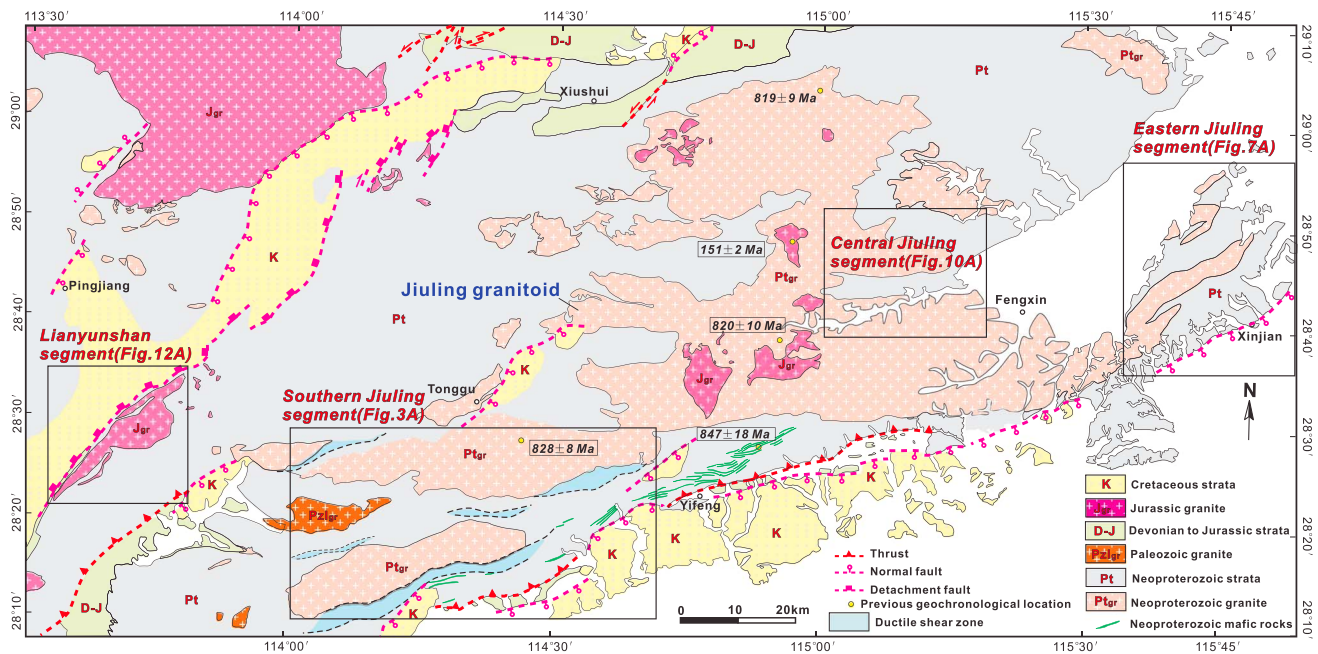


**Figure 2.** Tectonic map of the Jiuling and Lianyunshan domains of the central Jiangnan Orogen, simplified from published geological maps and locally modified on the basis of our field observations. See Figure 1b for location.

Shuangqiaoshan Group [Gao *et al.*, 2008; Wang *et al.*, 2008; Gao *et al.*, 2012], <840 Ma for the Xikou Group [Zhang *et al.*, 2010], 860–820 Ma for the Sibao/Fengjingshan/Lengjiayi Group [X. L. Wang *et al.*, 2007; Wang *et al.*, 2010; Gao *et al.*, 2010], and 820–750 Ma for the Banxi/Danzhu Group [Wang and Li, 2003; Gao *et al.*, 2007, 2011]. Notably, an angular unconformity outcrops extensively throughout the orogen, which separates the above rock sequences into two packages with contrasting structural styles. Rock sequences below the unconformity (>820 Ma) display tight linear, isoclinal, and overturned folds, thrusts, and penetrative cleavages, whereas those above the unconformity (<820 Ma) are flat-lying and exhibit open folds with rare cleavage development (e.g., SW [Dong *et al.*, 2015; X. L. Wang *et al.*, 2007]). The ~820 Ma flysch turbidites above the unconformity were the earliest continental rift deposits that marked the initial opening and rifting of the Nanhua Rift potentially related to the arrival of an ~825 Ma mantle plume [Li *et al.*, 1999; Wang and Li, 2003].

### 2.2. Magmatic Rocks and Ophiolites

Abundant Neoproterozoic, early Paleozoic and Mesozoic granitic intrusions have been identified in the Jiangnan Orogen [e.g., Li *et al.*, 2003; Yuan *et al.*, 2012; Shu *et al.*, 2014; Yao *et al.*, 2014]. The Neoproterozoic granitoids are characterized by penetrative foliations and asymmetric augen structures and have been previously classified as synorogenic and postorogenic granitoids [e.g., Li, 1999]. The synorogenic granitoids range in age from 835 to 800 Ma and are S-type intrusions that may be related to the Yangtze-Cathaysia collision [Yao *et al.*, 2014]. The postorogenic granitoids range from 820 to 780 Ma and include I-, S- and A-type intrusions that have been variously interpreted as the products of: crustal melting during continental rifting above a mantle plume [Li *et al.*, 2003; Zhong *et al.*, 2005; Wang *et al.*, 2010], or continental-margin magmatic arc development [Zhou *et al.*, 2002], or melting of a juvenile arc during orogenic collapse and lithospheric extension [Zheng *et al.*, 2008]. Andesite and mafic-ultramafic rocks of 860–810 Ma are abundant and occur as bedding-parallel sills within the Neoproterozoic strata (Figure 2) [Shu *et al.*, 2011; Y. Z. Zhang *et al.*, 2013; Yao *et al.*, 2014, 2015]. Geochemical data show that they have subduction-related arc signatures, although the direction of subduction is debated. Models include southeast directed subduction [Cawood *et al.*, 2013], northwest directed subduction [Guo *et al.*, 1989; Shu *et al.*, 1994; Shu, 2012; Yao *et al.*, 2015], and divergent double-sided subduction [Zhao, 2015] of the oceanic lithosphere intervening between the Yangtze and Cathaysia Blocks. Several early Paleozoic granitic plutons, dated at 402–440 Ma, are distributed in the southwestern margin of the Jiuling Massif [Charvet, 2013]. Geochemically, these plutons are peraluminous and their zircons show negative  $\epsilon_{\text{Hf}}(t)$  values [Shu *et al.*, 2014]. Mesozoic granitoids crop out extensively in the Lianyunshan Massif and are

rare in the Jiuling Massif (Figure 2) [Yuan *et al.*, 2012]. These granitoids display a porphyritic texture in the core with local mylonitic fabric development in the margin.

Dismembered ophiolites, including serpentized ultramafic-mafic rocks, wehrlite, gabbro, Na-rich diorite, spilite, keratophyre, siliceous limestone, and red jasper, occur predominantly along the eastern Jiangnan Orogen and assist in tracing the Shaoxing-Jiangshan-Pingxiang and Northeastern Jiangxi suture zones [e.g., Chen *et al.*, 1991; Shu *et al.*, 1994; Shu and Charvet, 1996; Charvet *et al.*, 1996; Zhang *et al.*, 2012; Shu, 2012]. Early Sensitive High-Resolution Ion Microprobe (SHRIMP) U-Pb and Sm-Nd isotopic dating gave Neoproterozoic ages (~0.97–0.83 Ga) for these ophiolites [Zhou *et al.*, 1989; Chen *et al.*, 1991; Li *et al.*, 1994; Zhang *et al.*, 2012]. However, their tectonic settings remain controversial; competing models emphasizing a small oceanic basin [Zhou *et al.*, 1989], an island arc [Chen *et al.*, 1991], interarc and continental-margin basins [Li *et al.*, 1994], and a back-arc basin [Zhang *et al.*, 2012] have been proposed. The ophiolites incorporate HP/LT blueschists ( $866 \pm 14$  Ma, K-Ar on glaucophane grains [Shu *et al.*, 1994]) in the Dongxiang-Dexing-Shexian fault zone. Similar ophiolitic assemblages are rarely preserved in the western Jiangnan Orogen and limit our ability to trace the suture zones westward. Despite this, Neoproterozoic oceanic subduction along the western Jiangnan Orogen is consistent with the presence of remnants of oceanic lithosphere, including ~900–850 Ma mafic-ultramafic rocks, normal mid-oceanic ridge basalt-type basalts, dolerites, pelagic flysch, limestone, and red colored chert in the Yuanbaoshan and Longsheng areas of the northern Guangxi Region [Zhou *et al.*, 2002; Yao *et al.*, 2014].

### 2.3. Controversies on the Timing of the Yangtze-Cathaysia Collision

Conventional wisdom explains the Jiangnan Orogen as the result of collision between the Yangtze and Cathaysia Blocks, as demonstrated by the aforementioned ophiolitic mélangé suites, island arc igneous rocks, syncollisional granites, high-pressure blueschists, and stratigraphic unconformity [e.g., Chen *et al.*, 1991; Li, 1994; Shu *et al.*, 1994; Charvet *et al.*, 1996; Li *et al.*, 1999, 2009]. However, the timing of collision remains controversial. Some researchers believe that the collision was the result of a diachronous ocean closure, lasting from 1.0 to 0.9 Ga based on U-Pb and  $^{40}\text{Ar}/^{39}\text{Ar}$  geochronology of syncollisional granitoids and metamorphism [e.g., Li *et al.*, 2002, 2007]. Others argue that the collision occurred during 0.85–0.82 Ga [X. L. Wang *et al.*, 2007; Wang *et al.*, 2013b; Zhao and Cawood, 1999, 2012; Yao *et al.*, 2014, 2015] or even younger in the early Paleozoic [Wang *et al.*, 2014; Yi *et al.*, 2014] based on detrital/magmatic zircon data for basement sequences, arc magmatism, and high-grade metamorphism. The recent finding of a buried Paleoproterozoic orogen beneath the western Jiangnan Orogen, identified using seismic reflection profiling, led Dong *et al.* [2015] to predict the amalgamation of the two blocks in the Paleoproterozoic, associated with the assembling of the Colombian supercontinent.

### 2.4. Previous Work on the Central Jiangnan Orogen

The central Jiangnan Orogen, composed of the continental Jiuling terrane and the Lianyunshan segment of the Northern Hunan terrane (Figure 2), is separated from the oceanic Huaiyu terrane of the eastern Jiangnan Orogen by the Northeastern Jiangxi suture zone (JXSZ in Figure 1). Together these continental, oceanic terranes and ophiolites have been explained as a Neoproterozoic trench-arc-back-arc marginal sea system across the Jiangnan Orogen [Shu and Charvet, 1996; Charvet *et al.*, 1996; Yao *et al.*, 2014]. Precambrian turbidite strata are widespread and consist of the Banxi (<820 Ma) and Lengjiayi/Shuangqiaoshan (860–820 Ma) Groups that are separated by an angular unconformity [Wang and Li, 2003]. In contrast to the extensive outcrops of Precambrian strata, Paleozoic and Mesozoic strata are sparsely preserved throughout the orogen (Figure 2). Devonian conglomerates rest unconformably on the Precambrian strata, implying significant uplifting and erosion during the early Paleozoic [Faure *et al.*, 2009; Charvet *et al.*, 2010]. Cretaceous red fluviatile and lacustrine sediments are accumulated along fault-bound NE trending extensional basins (Figure 2). Their deposition was coeval with regional magmatism and unroofing within an extensional tectonic setting [e.g., Zhou and Li, 2000; Shu *et al.*, 2009; Li *et al.*, 2014a, 2015a].

Tectonically, the central Jiangnan Orogen is a composite structural feature resulting from multiphase deformation including dip-slip and strike-slip faulting, ductile shearing, and double-verging folding. Previous investigations of structural fabrics yielded abundant data but contrasting interpretations. Shu and coworkers [Shu *et al.*, 1991, 1994] identified three deformation events; they related earliest top-to-the-south ductile thrusting to the Neoproterozoic Yangtze-Cathaysia collision and subsequent left-lateral ductile shearing and top-to-the-south brittle thrusting to early Paleozoic and Mesozoic intracontinental orogenesis, respectively. Chu and Lin [2014] distinguished four deformation events; they attributed early development of top-

to-the-NNW ductile thrusts (D1) and dextral shear fabrics (D2) to the early Paleozoic orogeny and subsequent NE trending folds (D3) and extensional fabrics (D4) to Triassic contraction during the Paleo-Pacific plate subduction and Cretaceous extensional collapse during slab rollback, respectively. Based on work in the eastern Jiangnan Orogen, *Xu et al.* [2015] attributed the D2 and D3 fabrics to synorogenic products resulting from the northward subduction of the Yunkai massif and the Yangtze-Cathaysia convergence, respectively. The contrasting structural interpretations are a direct consequence of limited field observations and sparse structurally constrained geochronological data.

### 3. Methodology

#### 3.1. Structural Geology

The regional-scale geological database comes from published geologic maps, which were partly updated with our own field observations and interpretations. At the outcrop scale, we measured foliation, lineation, and shear criteria (e.g., S-C fabrics, asymmetrical boudinages, and  $\sigma$  and  $\delta$  porphyroclasts) and collected oriented samples. For brittle structures, we measured fault planes and striations and recorded kinematic indicators (e.g., offset markers, fibrous minerals, and Riedel shears). Thin sections from oriented samples were used to document mineral associations and structures and to determine the kinematics and temperatures during deformation. Special attention is paid to the structural relation between outcrop structures and microscopic fabrics, because it is crucial for establishing the relative order of tectonic events and testing the geometric and kinematic compatibility among events [e.g., *Goodge et al.*, 1993].

#### 3.2. Zircon U-Pb Geochronology

Zircons were extracted using standard heavy liquid and magnetic techniques. Individual crystals were hand-picked, mounted in epoxy resin, and polished to about half thickness. Cathodoluminescence (CL) images were obtained using a JEOL scanning electron microscope to reveal internal structures and choose potential target sites for U-Pb analyses. The U-Pb dating on zircons was conducted by a laser ablation multicollector inductively coupled plasma-mass spectrometry (LA-MC-ICP-MS) coupled with a NewWave UP193FX ArF Excimer laser ablation system in the Tianjin Institute of Geology and Mineral Resources. All analyses were performed using a spot diameter of 35  $\mu\text{m}$ , at a repetition rate of 8–10 Hz and an energy density of 7–8 J/cm<sup>2</sup>. The standard GJ-1 and 91500 zircons were used to calibrate the U-Th-Pb ratios and absolute U abundance. U, Th, and Pb concentrations were calibrated by using <sup>29</sup>Si as an internal standard and NIST 610 as an external standard. The detailed analytical techniques and operating conditions are described in *H. K. Li et al.* [2010]. The age calculations and concordia diagrams were made using ISOPLOT 3.0 [*Ludwig*, 2003], with uncertainties on the weighted mean ages at 1 $\sigma$  error. Common Pb was corrected according to the method invoked by *Andersen* [2002].

#### 3.3. <sup>40</sup>Ar/<sup>39</sup>Ar Thermochronology

Muscovite, biotite, and K-feldspar mineral separates were extracted using heavy liquid and magnetic separation techniques. The mineral separates were irradiated for 3008 min in the nuclear reactor of Chinese Institute of Atomic Energy using the B4 hole. The intermittent flux of neutrons was  $2.65 \times 10^{13} \text{ n cm}^{-2} \text{ s}^{-1}$  and integrated flux of neutrons was  $4.78 \times 10^{18} \text{ n cm}^{-2}$ . The standard sample used to monitor neutron fluxes was the Chinese standard ZBH-25 (biotite) with an age of  $132.7 \pm 1.2 \text{ Ma}$  and a K content of 7.6%. Following neutron irradiation, argon isotopes were analyzed using MM-1200B Mass Spectrometer at the Ar-Ar Laboratory, Institute of Geology, Chinese Academy of Geological Sciences (Beijing). Mineral separates were step-heated in more than 10 steps at incrementally high power. Initially obtained data were corrected for discriminations, argon component, blanks, and irradiation-induced mass interference. Corrections for interfering Ar isotopes have been done using  $(^{36}\text{Ar}/^{37}\text{Ar})_{\text{Ca}} = 0.0002389$ ,  $(^{40}\text{Ar}/^{39}\text{Ar})_{\text{K}} = 0.004782$ , and  $(^{39}\text{Ar}/^{37}\text{Ar})_{\text{Ca}} = 0.000806$ . All <sup>37</sup>Ar were corrected for radiogenic decay; the decay constant used is  $\lambda = 5.543 \times 10^{-10} \text{ a}^{-1}$ . More detailed machine conditions and analytical procedures were described by *Chen et al.* [2002].

### 4. Structural Geology, Thermochronology, and Geochronology

Fieldwork was carried out in four study areas to document the geometry and kinematics of structures in the Jiuling and Lianyunshan domains of the central Jiangnan Orogen (Figure 2). This work was integrated with thermochronological and geochronological analyses of 11 samples.

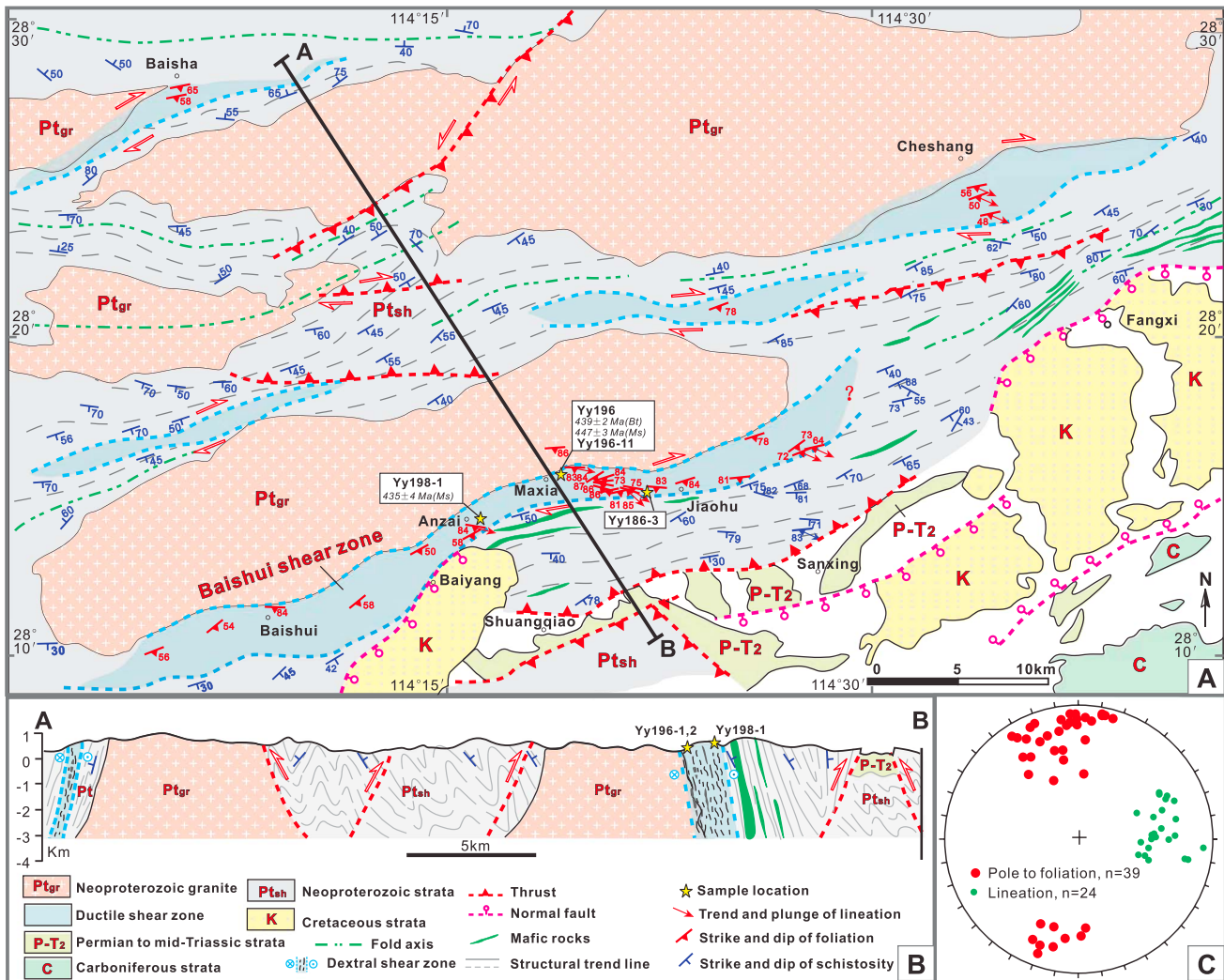


**Figure 3.** (a) Geologic map of the Southern Jiuling Segment (SJS), modified from published geological maps on the basis of our field measurements. See Figure 2 for location. Sample positions and their thermochronological results are also shown. Ms, muscovite; Bt, biotite. (b) Cross section A-B showing structural style of the SJS. (c) Equal-area lower hemisphere stereonet projection of measured structural data from the Baishui shear zone shows steeply ~E oriented foliations and gently east plunging lineations.

**4.1. The Southern Jiuling Segment**

**4.1.1. Structural Geology**

The Southern Jiuling Segment (SJS) is characterized by an ~40 km wide, ENE trending anticlinorium that consists of Neoproterozoic meta-sediments (Pt<sub>sh</sub>), granitoids (Pt<sub>gr</sub>), and Devonian to Cretaceous strata; these rocks have been juxtaposed along ductile shear zones, thrusts, and normal faults (Figures 3a and 3b). Multiple generations of structures record episodic transpressional, contractional, and extensional events.

**4.1.1.1. Ductile Shear Zones**

Several ENE striking high-strain ductile shear zones, originally interpreted as deformed migmatite zones [JBGMR (Hunan Bureau of Geology and Mineral Resources), 1979], are recognized. They are inherited zones of weakness that form the contacts between the Shuangqiaoshan Group and Neoproterozoic granitoids (Figure 3a). These zones are 1–3 km wide and progressively die out laterally into ENE trending folds involving Neoproterozoic strata (Figure 3a). Among them, the Baishui ductile shear zone is best exposed (Figure 3a). This zone truncates and attenuates the supracrustal rocks of the Shuangqiaoshan Group and involves the Jiuling granitoids to the north (Figures 3a and 3b). Shear-zone rocks are characterized by prominent S and L-S tectonite fabrics. The S

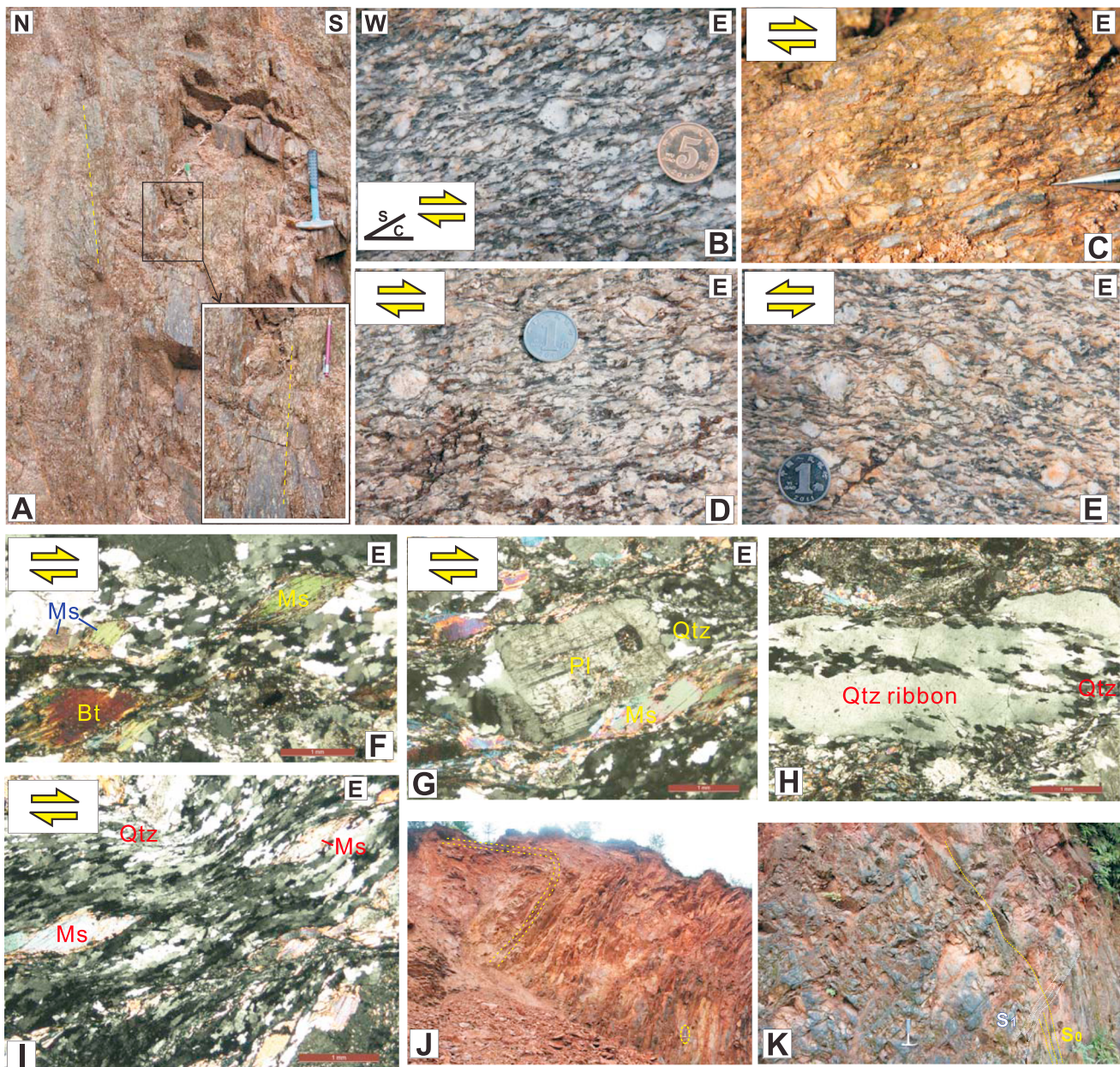


**Figure 4.** Field photographs and photomicrographs depicting main structural features in the Southern Jiuling Segment (SJS): (a) east oriented, steep-dipping foliation in the Baishui shear zone (location: ~3 km to the east of the Caotou Village). (b) Macroscopic S-C fabrics and (c)  $\sigma$ -type plagioclase porphyroclasts in mylonitic granites and gneisses consistently show dextral shear. (d and e) Two contrasting shear indicators at one locality (N28°16'09.82", E114°19'34.99"):  $\sigma$ -type feldspar porphyroclasts with asymmetrical tails indicate dextral and sinistral senses of shear, respectively. (f) Microscopic mica fishes and (g)  $\sigma$ -type plagioclase porphyroclast flanked by asymmetric elongated quartz wings confirm a dextral shear sense. (h and i) Elongated quartz ribbons show strain-free subgrains at their boundaries, recording dominant subgrain rotation (SGR) recrystallization. (j) Macroscopic folds with an upright limb in the schist (location: ~3 km to the northeast of the Shuangqiao Town). (k) Moderate-dipping axial cleavages (S1), interpreted as the attendant structures of tight folds, have structurally transposed the original bedding (S0) of the slate. Pl, plagioclase; Ms, muscovite; Bt, biotite; Qtz, quartz.

tectonites have a penetrative mylonitic foliation defined by preferably oriented, elongated quartz ribbons and aligned mica clusters. The mylonitic foliation strikes E-ENE and dips steeply to the south (Figure 4a). The L-S tectonites have in addition a mineral lineation defined by stretched quartz grains, aligned mica grains, and recrystallized tails on feldspar porphyroclasts. The lineations plunge shallowly to moderately to the east, indicating significant strike-slip shearing (Figure 3c). Shear-sense indicators, viewed in the x-z plane, include macroscopic S-C fabrics (Figure 4b) and  $\sigma$ -type feldspar porphyroclasts (Figure 4c), consistently illustrating a predominant

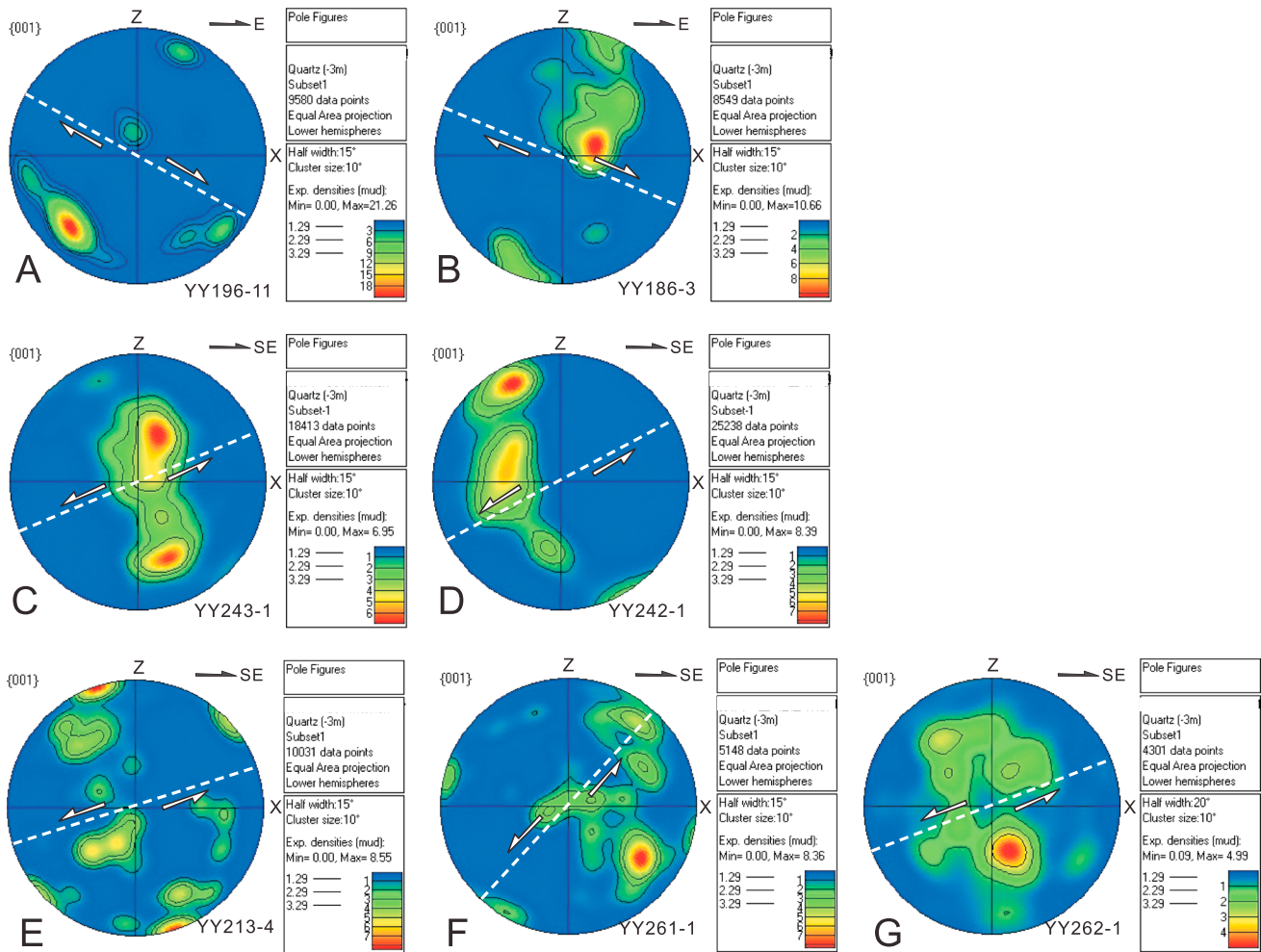


**Figure 5.** Quartz c-axis fabric diagrams (lower hemisphere, equal area) of mylonitic rocks from the Southern (a and b), the Eastern (c and d), and the Central (e–g) Jiuling segments. Structural directions: x, parallel to the lineation; z, normal to the foliation.

dextral shear sense. Despite this, at one locality (N28°16'09.82", E114°19'34.99"), contrasting shear indicators are observed;  $\sigma$ -type feldspar porphyroclasts with asymmetrical tails indicate both dextral (Figure 4d) and sinistral (Figure 4e) senses of shear. Although fabrics indicative of sinistral shear are less prominent, their apparent incompatibility with dextral shear fabrics testifies to the existence of two distinct deformation events. However, their relative chronology cannot be determined due to the lack of an outcrop containing the overprinting relationship between the two shear fabrics.

Microstructures, such as mica fishes (Figure 4f) and  $\sigma$ -type plagioclase porphyroclast flanked by asymmetric elongated quartz wings (Figure 4g), confirm a dextral shear motion. Quartz represents the most common mineral in the shear zone. It occurs as elongated ribbons that are recrystallized and have subgrains along their boundaries (Figures 4h and 4i). The subgrains are small, polygonal, and display strong undulose extinction (Figures 4h and 4i), indicative of subgrain rotation (SGR) recrystallization. Quartz c-axis fabrics on two oriented mylonites (samples YY196-11 and YY186-3; see Figure 3a for their locations) record asymmetric, type I crossed girdles [e.g., Lister, 1977] (Figures 5a and 5b) that are consistent with right-lateral deformation under plane strain simple shear conditions [e.g., Etchecopar and Vasseur, 1987]. Quartz lattice-preferred orientation (LPO) patterns exhibit dominant basal  $\langle a \rangle$  slip in sample YY196-11 (Figure 5a) and mixed prime  $\langle a \rangle$  and basal  $\langle a \rangle$  slip in sample YY186-3 (Figure 5b), respectively. These recrystallized microstructures and LPO patterns consistently indicate that dextral shearing commenced under upper greenschist facies conditions at temperatures of 400–500°C [Stipp et al., 2002].

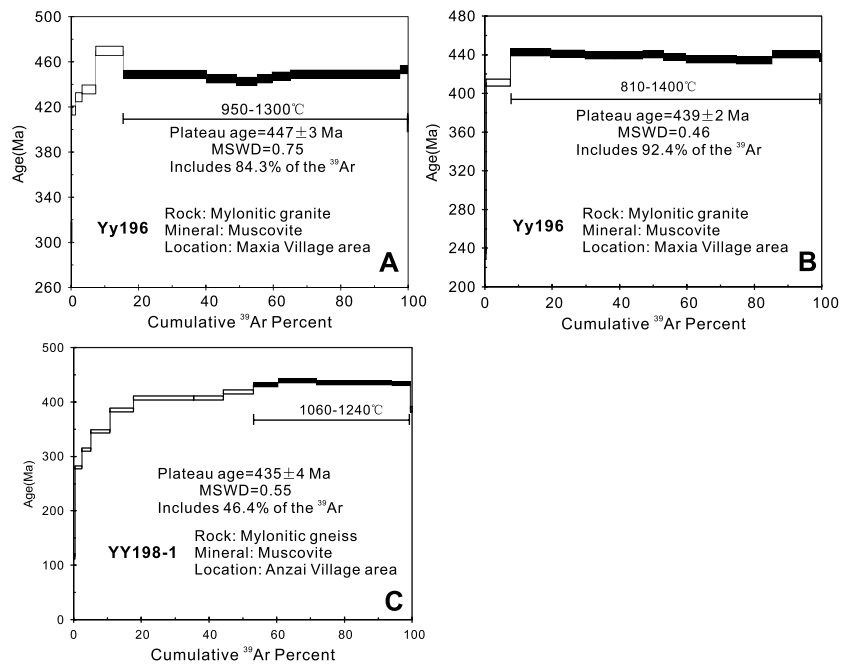


**Figure 6.** Biotite and muscovite  $^{40}\text{Ar}/^{39}\text{Ar}$  data for mylonitic gneisses and granites from the Baishui shear zone. MSWD, mean square of weighted deviates.

#### 4.1.1.2. Brittle Thrusts and Folds

At shallower structural levels, the Neoproterozoic sediments exhibit lower strain and are characterized by pervasive mesoscopic folds and brittle thrusts (Figure 3a). The folds affect a preexisting schistosity (Figure 4j). Fold limbs locally show brittle slickensides oblique to a weakly developed lineation, suggesting that early ductile strain was subsequently subjected to a brittle overprint. The folds trend ENE-WSW and have half-wavelengths ranging from tens of centimeters to several hundreds of meters (Figure 3a). They are tight to open and, in high-strain areas, are accompanied by a well-developed axial cleavage that dips moderately or steeply to the NNW or SSE, and which transposes the original bedding/schistosity (Figure 4k). The folds and associated cleavage reflect regional NNW-SSE contraction.

Arrays of ENE striking, moderately dipping brittle thrusts place Neoproterozoic metasedimentary rocks over Permian to mid-Triassic carbonates along the southern margin of the SJS (Figure 3a) and indicates that the thrusting postdates mid-Triassic sedimentation. Based on the concordant orientation of the thrusts, we assume that they are subparallel imbricate thrusts that branch from a midcrustal subhorizontal décollement zone [Chu and Lin, 2014]. The thrusts die out laterally into the above-described folds, indicating that the folds and thrusts are coeval and kinematically and genetically linked.

#### 4.1.2. $^{40}\text{Ar}/^{39}\text{Ar}$ Thermochronology

Two mylonitic samples (YY196 and YY198-1) were collected from an east striking portion of the Baishui ductile shear zone that is characterized by dextral kinematic indicators (Figure 3a). These samples were dated using  $^{40}\text{Ar}/^{39}\text{Ar}$  thermochronology to provide time constraints on dextral shearing.

Sample YY196 is a mylonitic granite that contains biotite, muscovite, K-feldspar, plagioclase, and quartz. Mica-fish-shaped muscovites yield a weighted mean age of  $447 \pm 3$  Ma (mean square of weighted deviate (MSWD) = 0.75), including seven steps (Steps 6–12) and 84.3%  $^{39}\text{Ar}$  (Figure 6a and Table S1 in the supporting information). The coexisting biotites give a younger weighted mean age of  $439 \pm 2$  Ma (MSWD = 0.46), including 10 steps (Steps 3–12) and 92.4%  $^{39}\text{Ar}$  (Figure 6b and Table S1). Their isochron ages are  $450 \pm 8$  Ma (MSWD = 4.8) and  $438 \pm 6$  Ma (MSWD = 3.7), respectively, both with near-atmospheric initial  $^{40}\text{Ar}/^{39}\text{Ar}$  values.

Sample YY198-1 is a mylonitic gneiss that contains muscovite, biotite, plagioclase, and quartz. Muscovite concentrates record a weighted mean age of  $435 \pm 4$  Ma (MSWD = 0.55) (Figure 6c), virtually identical to its isochron age of  $432 \pm 7$  Ma, with a near-atmospheric initial  $^{40}\text{Ar}/^{36}\text{Ar}$  ratio. These ages are defined by ~46.4%  $^{39}\text{Ar}$  release for four successive heating steps (Steps 9–12) at  $2\sigma$  level of uncertainty (Table S1).

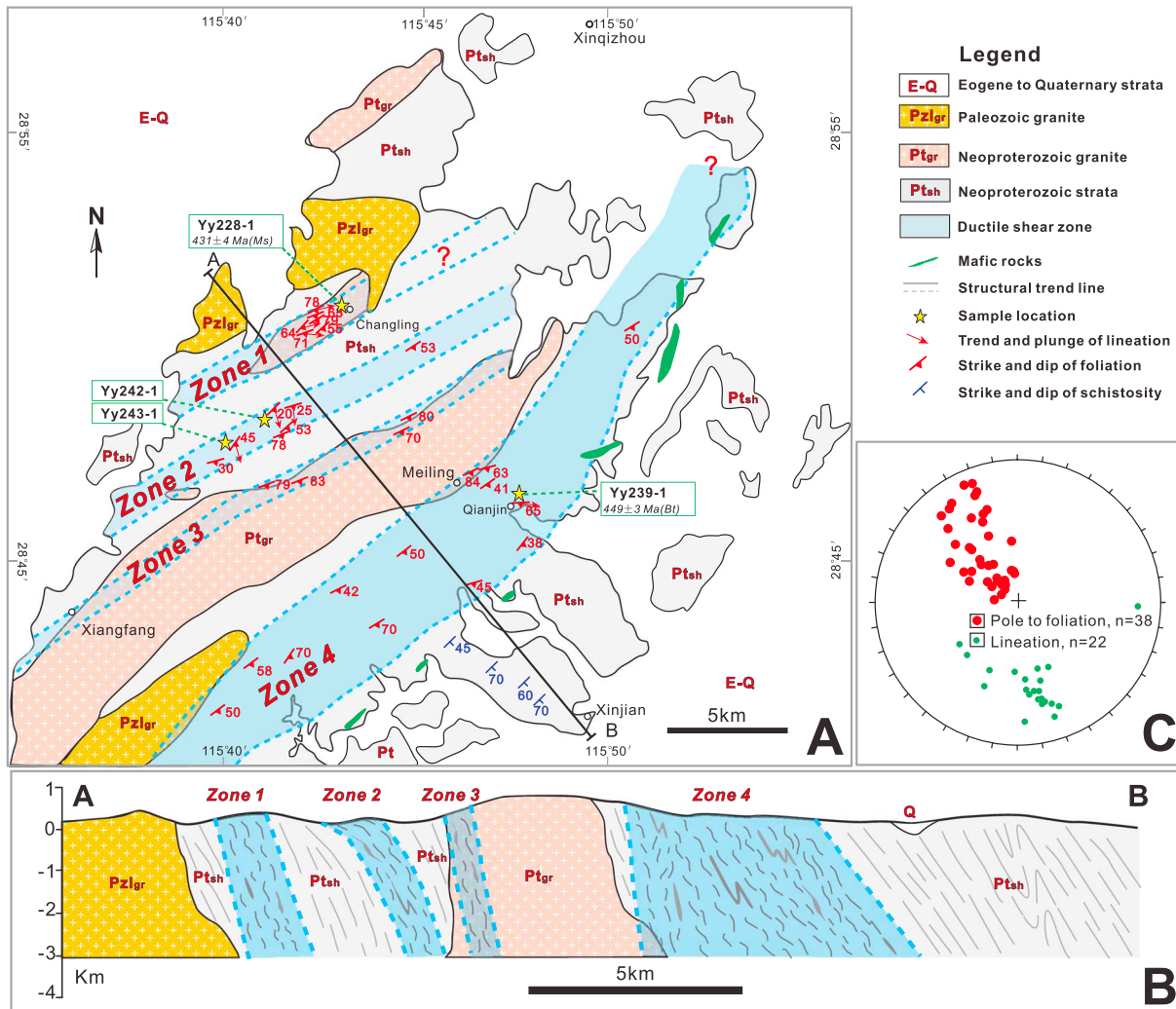


**Figure 7.** (a) Geologic map of the Eastern Jiuling Segment (EJS), modified from published geological maps based on our field measurements. See Figure 2 for location. Sample positions and their thermochronological results are also shown. Ms, muscovite; Bt, biotite. (b) Cross section A-B showing structural style of the EJS. (c) Stereonet projection of our measurements shows NE-SW foliations and SE plunging lineations for zones 1–4.

## 4.2. The Eastern Jiuling Segment

### 4.2.1. Structural Geology

The main lithological units of the Eastern Jiuling Segment (EJS) include the Shuangqiaoshan meta-sediments (Pt<sub>sh</sub>) and Neoproterozoic and early Paleozoic granitoids (Pt<sub>gr</sub> and Pz<sub>gr</sub> in Figure 7a). Strain partitioning within the EJS gave rise to high-strain (ductile shear) zones that grade abruptly into fold and thrust zones of moderate to low strain with weak or no ductile fabric development. Four high-strain ductile shear zones (zones 1–4 from the NE to SW, respectively) are identified (Figures 7a and 7b).

The penetrative foliation in the four zones constantly strikes NE-SW and dips to the SE (Figure 7a) and is locally folded about a subhorizontal NE trending axis, with dip angles varying from >70° (Figure 8a) to <25° (Figure 8b). A stretching lineation is locally well developed, especially in zones 1 and 2; it plunges to the SE and SSE, at an ~40°–80° angle to associated foliation trend (Figure 8c). Mesoscopic kinematic criteria, such as S-C fabrics, are particularly well developed in the coarse-grained biotite gneiss of zones 1 and 2. C planes (shear planes) subparallel to the shear zone margins are defined by segregated quartz and mica aggregates. S planes (schistosity), defined by quartz ribbons and aligned biotite grains, make an ~30° angle to C planes, revealing top-to-the-northwest oblique thrust asymmetry with a sinistral strike-slip component (Figures 8d and 8e). Under the microscope, quartz porphyroclasts are elongate, boudinaged, and show

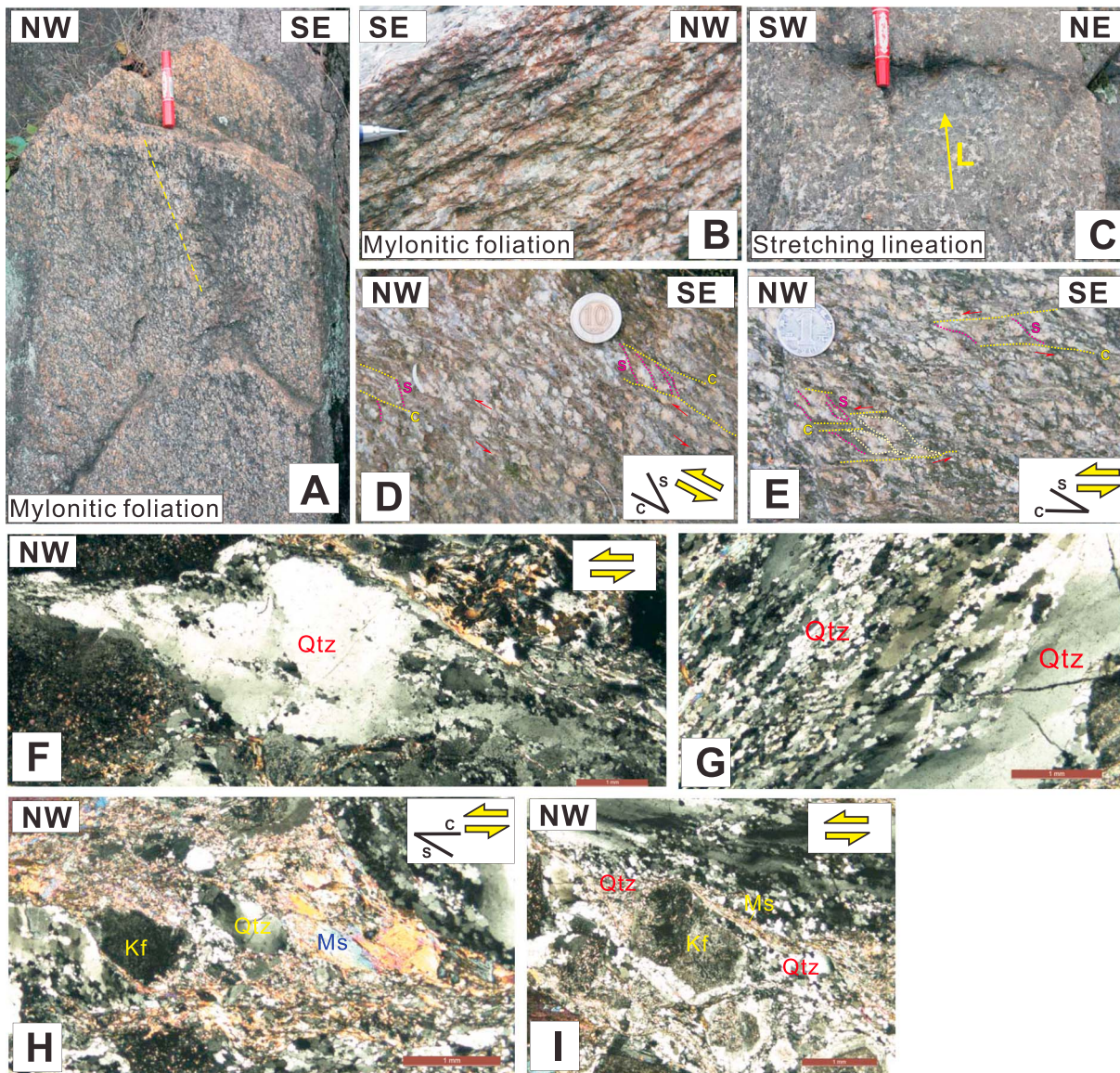


**Figure 8.** Field photographs and photomicrographs depicting main structural features in the Eastern Jiuling Segment: (a) NE oriented, steep-dipping foliation in zone 1. (b) NE oriented, shallow-dipping foliation in zone 2. (c) SSE-NNW stretching lineation in zone 2, perpendicular to regional foliation trend. (d) and (e) Macroscopic S-C fabrics in biotite gneisses attest for top-to-the-northwest thrust shear in zone 2. (f) Asymmetrically elongated quartz porphyroclasts show undulatory extinction and core-and-mantle structures, diagnostic of bulging (BLG) recrystallization. (g) Elongated quartz ribbons show recrystallized subgrains, diagnostic of subgrain rotation (SGR) recrystallization. (h) S-C fabrics and (i) winged feldspar porphyroclast record a northwest directed thrust shear. Kf, K-feldspar; Ms, muscovite; Bt, biotite; Qtz, quartz.

undulatory extinction, core-and-mantle structures (Figure 8f) and recrystallized subgrains (Figure 8g), diagnostic of bulging (BLG) and subgrain rotation (SGR) recrystallization. Muscovite and biotite occur asymmetrically and form trails of pull-apart fragments in S-C fabrics (Figure 8h). Feldspar porphyroclasts are rigid, rotated, and flanked by quartz-filled pressure shadows (Figure 8i). These microstructures show asymmetry that reveals a northwest directed (oblique) thrust shear, consistent with mesoscopic kinematic criteria.

We analyzed quartz c-axis fabrics on two oriented mylonites (samples YY243-1 and YY242-1) from zone 2 (Figure 7a). These samples record asymmetric single girdles that confirm a consistent top-to-the-NW, or thrust, motion during noncoaxial ductile flow (Figures 5c and 5d). The pole figures of quartz c-axis suggest the activation of rhomb  $\langle a \rangle$  and basal  $\langle a \rangle$  slip systems in samples YY243-1 and YY242-1 (Figures 5c and 5d),

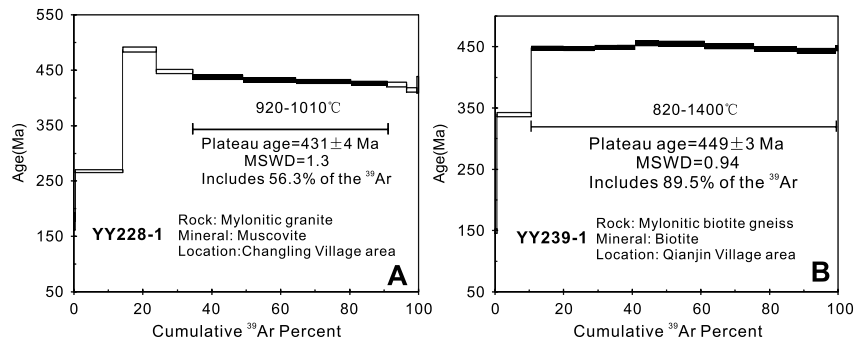


**Figure 9.** Biotite and muscovite  $^{40}\text{Ar}/^{39}\text{Ar}$  data for mylonitic gneisses and granites from the Eastern Jiuling Segment. MSWD, mean square of weighted deviates.

respectively. To sum up, recrystallized microstructures and quartz *c*-axis fabrics suggest ductile deformation in the four zones under greenschist-facies metamorphic conditions at temperatures of 350–450°C.

**4.2.2.  $^{40}\text{Ar}/^{39}\text{Ar}$  Thermochronology**

Sample YY228-1 is a mylonitic granite from zone 1 that contains a steeply SE dipping foliation and a moderately south plunging lineation associated with oblique thrust shearing. Mica-fish-shaped muscovites yield a plateau at  $431 \pm 4$  Ma covering 56.3% of the total  $^{39}\text{Ar}$  (Figure 9ba and Table S1), virtually identical to an isochron age of  $426 \pm 42$  Ma (MSWD = 2.5).

Sample YY239-1 is a mylonitic biotite-bearing gneiss from zone 4 that preserves a steeply SE plunging lineation and thrust shear fabrics. Asymmetrically aligned biotites yield a well-defined plateau at  $449 \pm 3$  Ma covering 89.5% of the total  $^{39}\text{Ar}$  (Figure 9b and Table S1) and a consistent isochron age of  $450 \pm 5$  Ma (MSWD = 6.5) with a near-atmospheric initial  $^{40}\text{Ar}/^{36}\text{Ar}$  value of  $286 \pm 58$ .

**4.3. The Central Jiuling Segment**

The Central Jiuling Segment (CJS) is covered by Neoproterozoic Shuangqiaoshan metasediments and intruded by a large volume of granodiorite (Figures 10a and 10b). Granodiorite makes up the bulk of the Jiuling Massif and has been interpreted as resulting from crustal anatexis caused by conductive heating above a mantle plume [Li *et al.*, 2003]. SHRIMP zircon U-Pb geochronology indicates crystallization at

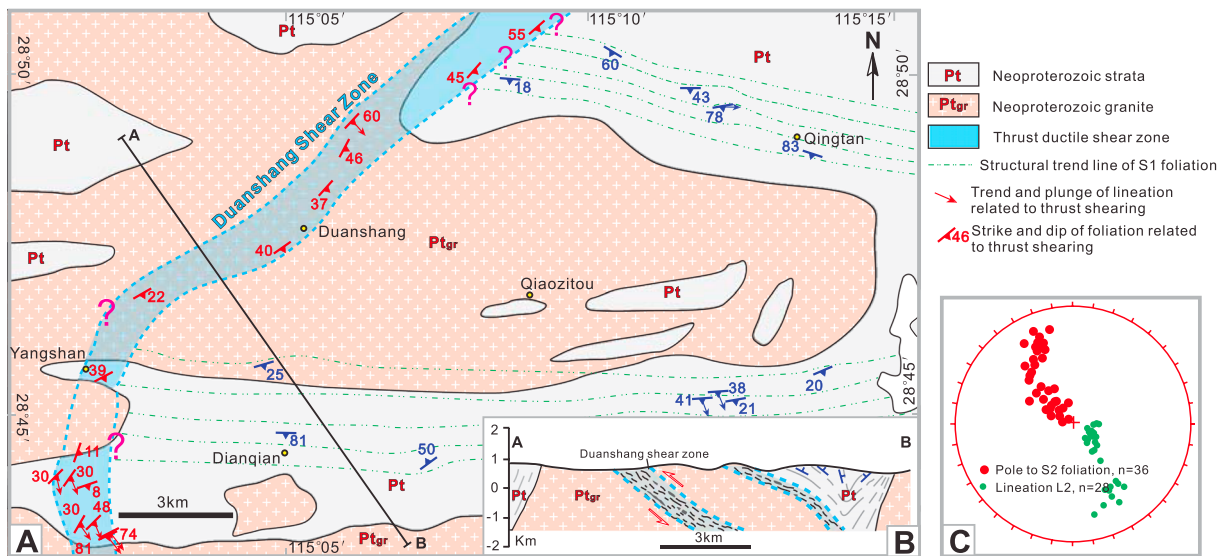


**Figure 10.** (a) Geologic map of the Central Jiuling Segment (CJS), modified from published geological maps based on our field measurements. See Figure 2 for location. (b) Cross section A-B showing structural style of the CJS. (c) Stereonet projection of our measurements shows NE oriented foliations and SE plunging lineations for the Duanshang ductile shear zone.

~828 Ma [Zhong *et al.*, 2005]. Two distinct generations of mylonitic foliation ( $S_1$  and  $S_2$ ) and stretching lineation ( $L_1$  and  $L_2$ ) are identified. However, in field sections, their order of development has not been determined due to a lack of quality outcrop.

The  $S_1$  foliation strikes E-W, parallel to that in the SJS. The related  $L_1$  stretching lineation is locally developed and plunges moderately to the east in the metasediments; it is less evident in the core of the granodiorite (Figure 10a). Kinematic criteria, including mica fish and  $\sigma$ -type feldspar porphyroclasts, attest to top-to-the-N(N)W oblique thrust shear. Quartz porphyroclasts are elongate and boudinaged with asymmetric tails. Feldspar porphyroclasts are rotated and have brittle fractures and microfaults. These fabrics are similar to those that characterize the SJS. In addition to the ~E striking shear fabrics, field observations document a NE-striking, high-strain ductile shear zone (Duanshang shear zone) (Figures 10a and 10b) characterized by a well-developed NE-SW foliation ( $S_2$ ) and a dip-slip stretching lineation ( $L_2$ ). Recrystallized quartz ribbons and micaceous aggregates define the  $S_2$  foliation.  $S_2$  dips shallowly to steeply ( $21^\circ$ – $81^\circ$ ) to the southeast (Figures 10c and 11a and 11b). The pronounced  $L_2$  lineation is defined by the elongate quartz rods and preferred orientations of feldspar and mica grains.  $L_2$  trends perpendicular to the strike of  $S_2$  and plunges gently to steeply toward the SSE (Figures 9b and 11c). Locally abundant mesoscopic kinematic indicators such as S-C fabrics indicate a top-to-the-NW thrust shear sense (Figure 11d). Thrust sense shear is also recorded by microscopic structures including mica fish (Figures 11e and 11f), S-C fabrics (Figure 11f), and quartz-filled pressure shadows around large plagioclase porphyroclasts (Figures 11g and 11h).

Dynamic recrystallization of quartz yielded large grains characterized by undulose extinction and lobed boundaries, forming cores surrounded by strain-free subgrains (Figure 11i). These textures are consistent with mixed grain-boundary migration (GBM) and subgrain-rotation (SGR) recrystallization. Quartz c-axis fabrics in three thrust-related mylonite samples show well-defined asymmetric single girdles. Their asymmetries confirm that noncoaxial ductile flow was in a top-to-the-NW, or thrust, motion (Figures 5e–5g). The pole figures of quartz c-axis suggest the activation of basal  $\langle a \rangle$  slip system in samples YY213-4 and YY261-1 (Figures 5e and 5f), and rhomb  $\langle a \rangle$  slip system in sample YY262-1 (Figure 5g). These quartz recrystallized structures and LPO patterns demonstrate greenschist facies metamorphic conditions, at temperatures of 350–500°C.

#### 4.4. The Lianyunshan Segment

##### 4.4.1. Structural Geology

The Lianyunshan segment lies 20 km west of the Jiuling massif and is characterized by a low-angle detachment fault (the Hengshan detachment fault) that separates a hanging wall Cretaceous supradetachment basin from an exhumed footwall composed of Neoproterozoic metamorphic rocks and Mesozoic granitoids (Figure 12a). Structural features, including ductile foliations and lineations, thrusts, folds, and normal faults, are described below.

##### 4.4.1.1. Ductile Shear Deformation

Two 1 km thick east striking, steeply south dipping ductile shear zones (zones 1 and 2) develop in the central part of the Lianyunshan segment. They involve and attenuate Neoproterozoic granitic gneisses and are truncated by undeformed Mesozoic granitoids (Figure 12a). The two shear zones are characterized by felsic minerals, mica clusters, and elongate quartz ribbons that exhibit flow features, and which together define a mylonitic foliation. These steeply dipping mylonites (Figure 13a) have a shallowly ( $\sim 20^\circ$ ) west plunging mineral lineation (Figure 12b). Asymmetric tails on feldspar porphyroclasts and shear bands from mylonitic orthogneiss indicate a consistent sinistral sense of shear (Figures 13b and 13c). Upright tight to isoclinal, rootless folds with axes parallel to the lineation are common, attesting to localized bulk high shear-strain (Figure 13d). Ductile flow, elongate quartz grains with high aspect ratios, and brittle fractures in rotated feldspar porphyroclasts (Figures 13b and 13c), indicate sinistral shearing at greenschist facies conditions. Zone 2 is distinguished by pervasive migmatization. Migmatitic leucosomes are boudinaged, tightly folded, and transposed into parallelism with regional  $S_1$  foliation (Figure 13e), implying that sinistral shearing commenced after, or during migmatization. Foliated orthogneiss and the migmatites are cross-cut by undeformed, post-tectonic pegmatite veins (Figure 13f).

Compared to the map-scale dextral and thrust shear zones in the Jiuling Massif, the two sinistral shear zones are small and their westward continuations are obscured by Jurassic plutonism (Figure 12a). Mineral deformation behaviors in the two zones display a marked similarity to the sinistral fabrics observed at Site 196

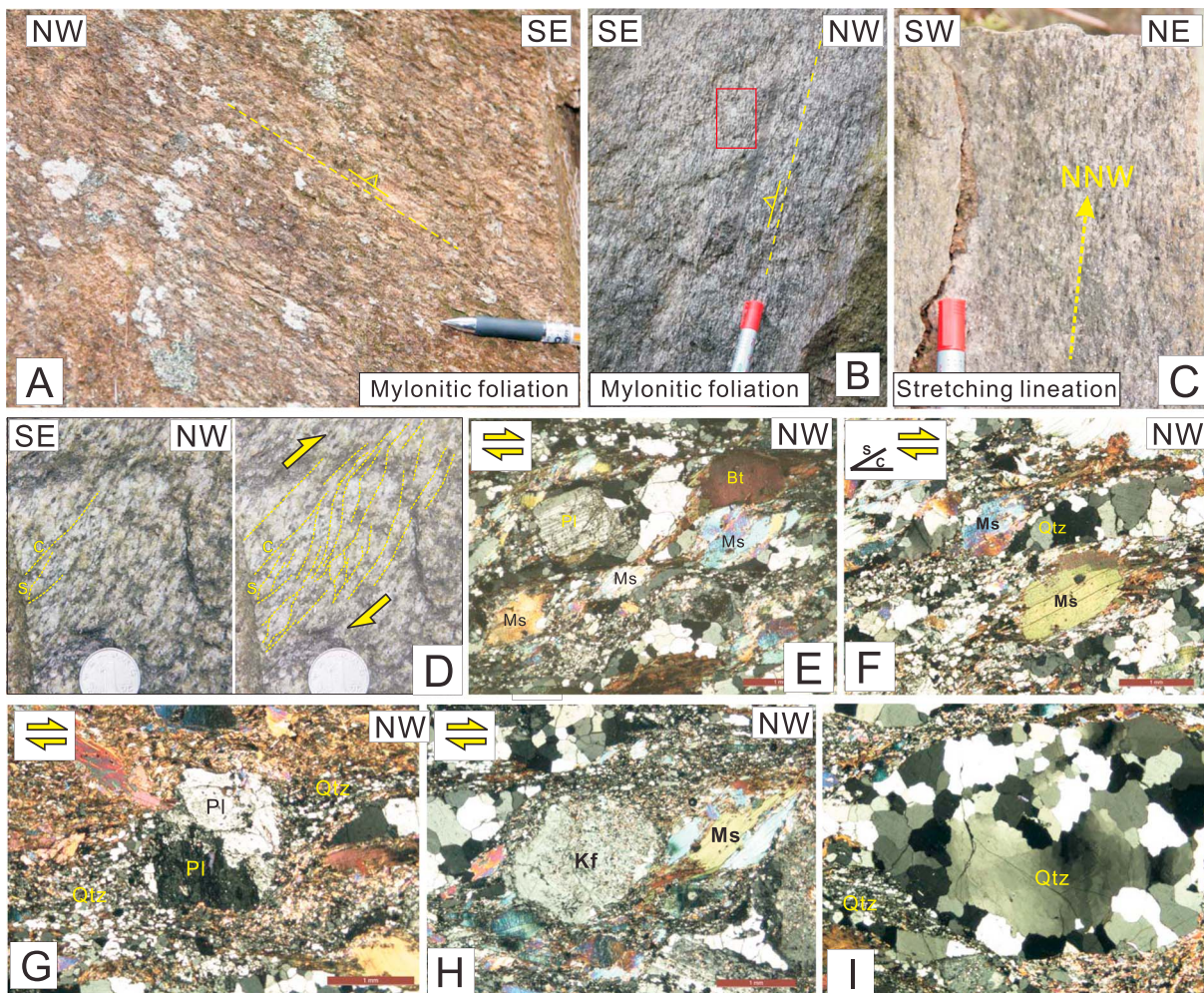


**Figure 11.** Field photographs and photomicrographs depicting main structural features in the Central Jiuling Segment: (a) NE oriented, shallow-dipping foliation ( $S_2$ ) in mylonitic schists. (b) NE oriented, steep-dipping foliation ( $S_2$ ) in mylonitic granites. (c) NNW-SSE stretching lineation ( $L_2$ ) in mylonitic granites. (d) Mesoscopic S-C fabrics indicate a top-to-the-NW thrust shear sense. (e–h) Microscopic structures, including asymmetric mica fishes (e and f), S-C fabrics (f), and quartz-filled pressure shadows around large plagioclase porphyroclasts (g and h) show a consistent top-to-the-NW thrust shear sense. (i) Quartz grains with lobed boundaries constitute a large core that is surrounded by smaller strain-free subgrains, illustrating mixed grain-boundary migration (GBM) and subgrain-rotation (SGR) recrystallization. Pl, plagioclase; Ms, muscovite; Bt, biotite; Qtz, quartz; Kf, K-feldspar.

(Figure 4e) in the SJS, enabling the possibility that they were contemporaneous structures induced by ~NE-SW transpression. However, the outcrops with east striking sinistral fabrics are rare and discontinuous. The significance of the sinistral shear remains unclear. We speculate that the outcrops with sinistral shear may represent (1) remnants of earlier structures with the majority having been erased by subsequent dextral and thrust deformation; (2) local traces of reverse shearing that develops during mylonitic shearing, associated with low-grade metamorphism [e.g., Hippertt and Tohver, 1999]; or (3) local reversals of dextral fabrics, due to the refolding of earlier dextral shear zones about an axis parallel to the lineation trend [e.g., Holcombe et al., 1991].

#### 4.4.1.2. Folds and Brittle Thrusts

Pervasive open to tight folds involve the Neoproterozoic meta-sediments. Within the metasediments, the primary bedding is hard to distinguish due to low-grade metamorphic overprinting, and the folded planar structure is a metamorphic schistosity. Across mapping transect A-B-C, two distinct structural domains (Domains 1 and 2) are juxtaposed by a NE striking, steeply SE dipping, dextral oblique-slip brittle thrust fault (Figure 12a). Domain 1 is an ~8 km wide zone that is separated from the Pingjiang basin to the NW by the WSW striking, shallow-dipping Hengshan detachment fault (Figure 12c). A variably dipping, migmatitic schistosity characterizes Domain 1 and defines NW vergent, upright to inclined folds (Figure 13g). Lower hemisphere equal-area projections of poles to schistosity yield a fold axis that plunges ~42° to the WSW (Figure 12d) and implies

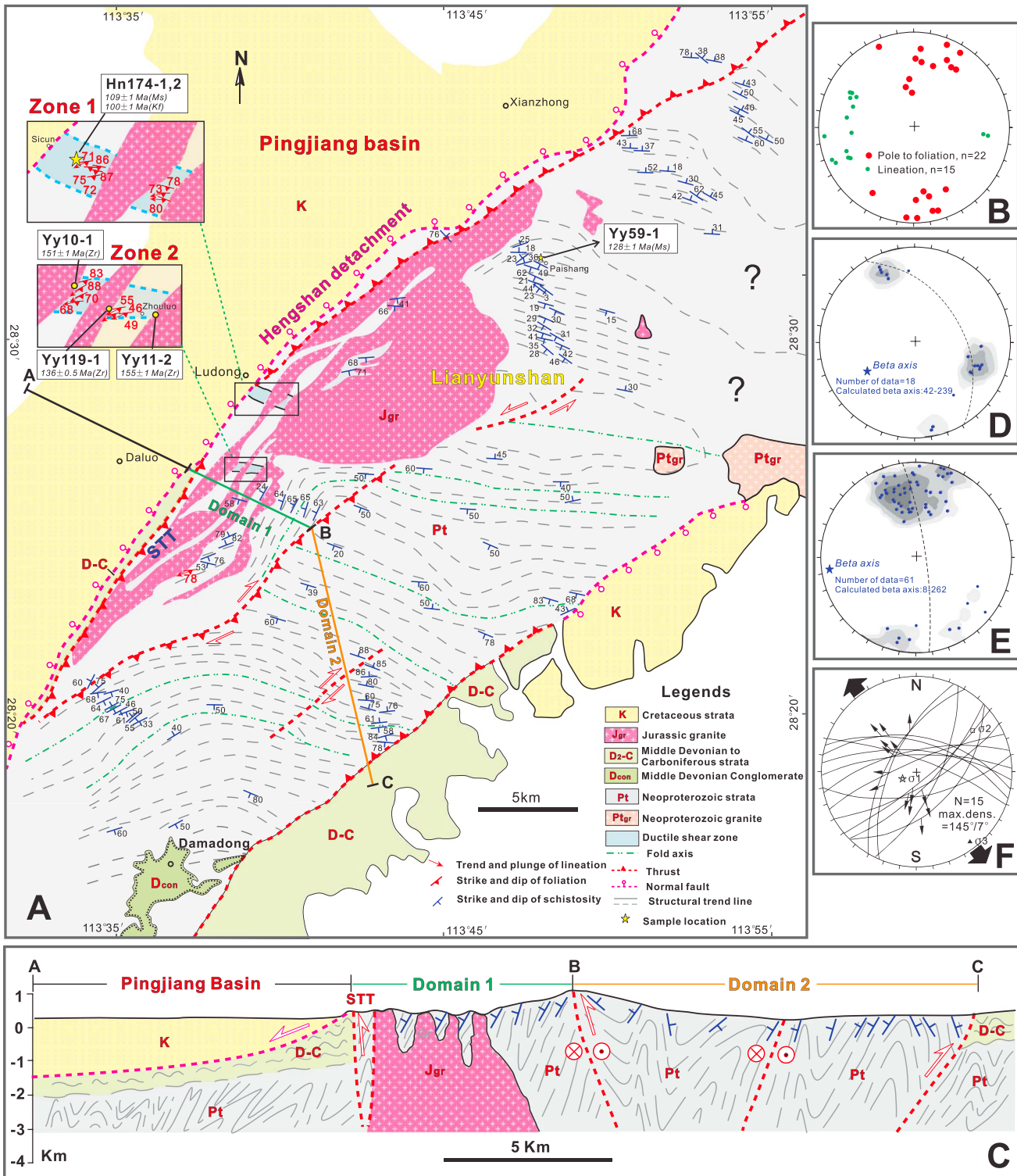


**Figure 12.** (a) Geologic map of the Lianyunshan Segment, modified from published geological maps based on our field measurements. See Figure 2 for location. Sample positions and their thermochronological results are also shown. (b) Stereonet projection of our measurements shows east oriented, steep-dipping foliations and shallowly plunging lineations for zones 1 and 2. (c) Cross section A-B showing structural style of the Lianyunshan Segment. (d and e) Lower hemisphere equal-area projections of the poles to schistosity show that the average fold axis is oriented SWS-NNE and plunges to WNW-W in Domains 1 and 2, both compatible with NNW-SEE contraction. (f) Stereonetic plots of brittle normal faults within the supradetachment basin document NW-SE extension.

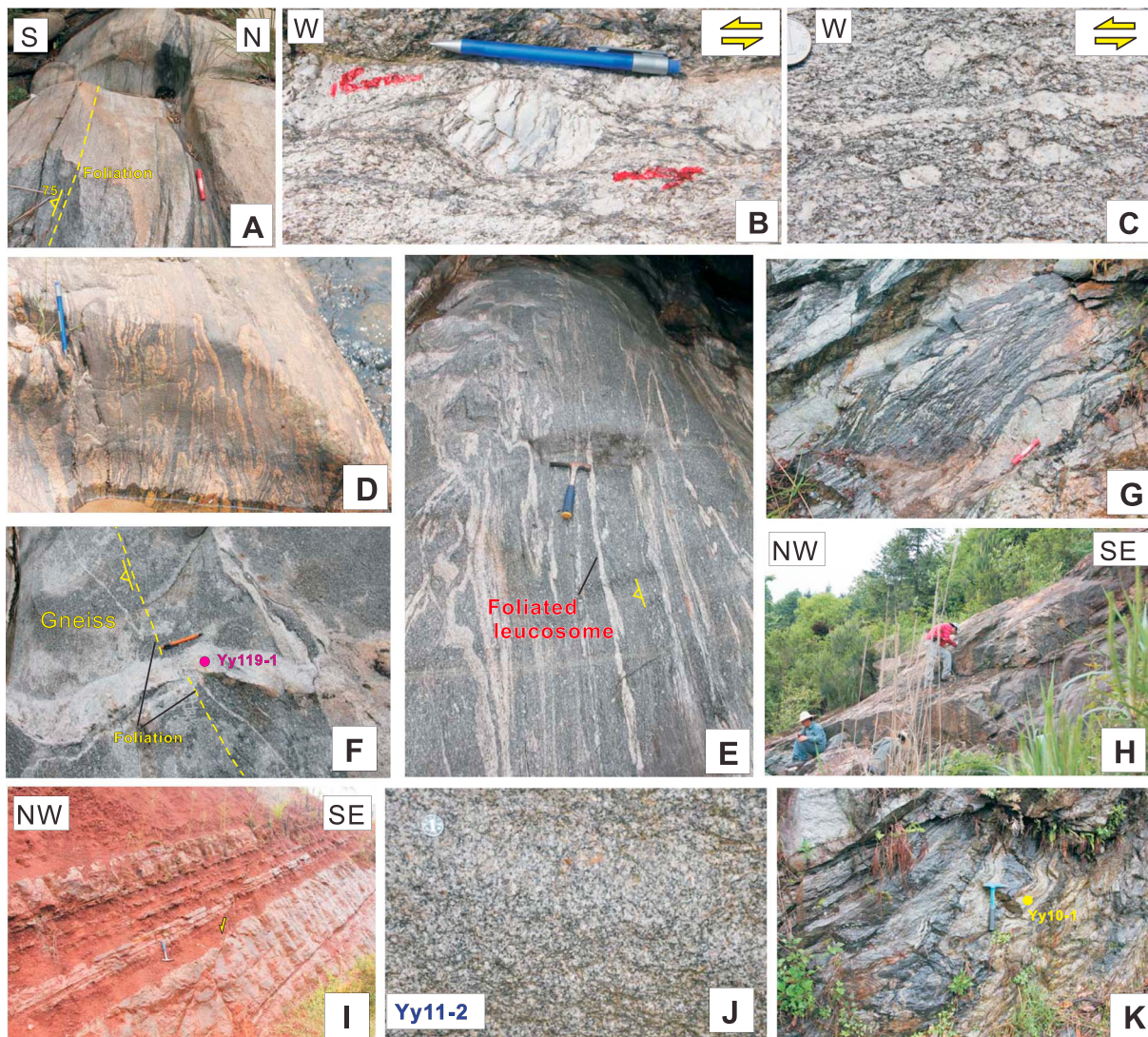


**Figure 13.** Field photographs showing main structural features in the Lianyunshan Segment: (a) east oriented, steep, south dipping foliation in mylonitic gneiss from zone 1. (b and c) Feldspar porphyroclasts with asymmetric tails and shear bands from mylonitic orthogneisses in zones 1 and 2 suggest a consistent sinistral shear sense. (d) Rootless folds with axes parallel to the lineation attest for localized bulk shear-strain intensities in zone 1. (e) Leucosomes from zone 2 are boudinaged, tightly folded that transposed into parallelism with regional  $S_1$  foliation. (f) Undeformed pegmatite veins crosscutting the foliated orthogneiss and leucosomes. (g) NW vergent inclined folds in Domain 1, accompanied by migmatization. (h) Low-angle, west dipping detachment fault, beneath which mineralized breccias are observed. (i) A brittle, northwest dipping normal fault in the supradetachment basin that is kinematically compatible with NW-SE extension. (j) Undeformed, cross-cutting monzogranites (sample YY11-2) emplaced at the easternmost end of zone 1. (k) A granitic melt (sample YY10-1) that intruded along the folded schistosity within the gneisses.

NNW-SSE contraction during folding. Locally, the contraction was accommodated by pressure solution and gave rise to axial planar cleavage that dips steeply to the NW. Along the westernmost part of Domain 1, the NE striking Shantian thrust (STT in Figure 12a) juxtaposes folded metasediments over Devonian carbonates, implying a post-Devonian age for the thrusting.

Domain 2 lies to the east of Domain 1. The boundary is a NE striking, steeply SE dipping thrust that places less migmatitic rocks of Domain 2 over the east margin of Domain 1. Domain 2 folds are arcuate in map view; fold traces are convex toward the NNW (Figure 12a). Measurements of folded schistosity yield a shallowly WSW plunging average fold axis (Figure 12e), reflecting ~N-S contraction. At the two ends, the WSW plunging folds are cut by two NE-striking thrusts, indicating that the folding predated the NW and SE directed thrusting. To the south of Domain 2, previous geological mapping [HBGMR (*Hunan Bureau of Geology and Mineral Resources*), 1976] shows that the folds are unconformably overlain by Middle Devonian conglomerates ( $D_{con}$ ) in the Damadong area (Figure 12a), indicating a pre-Devonian age for the folding.

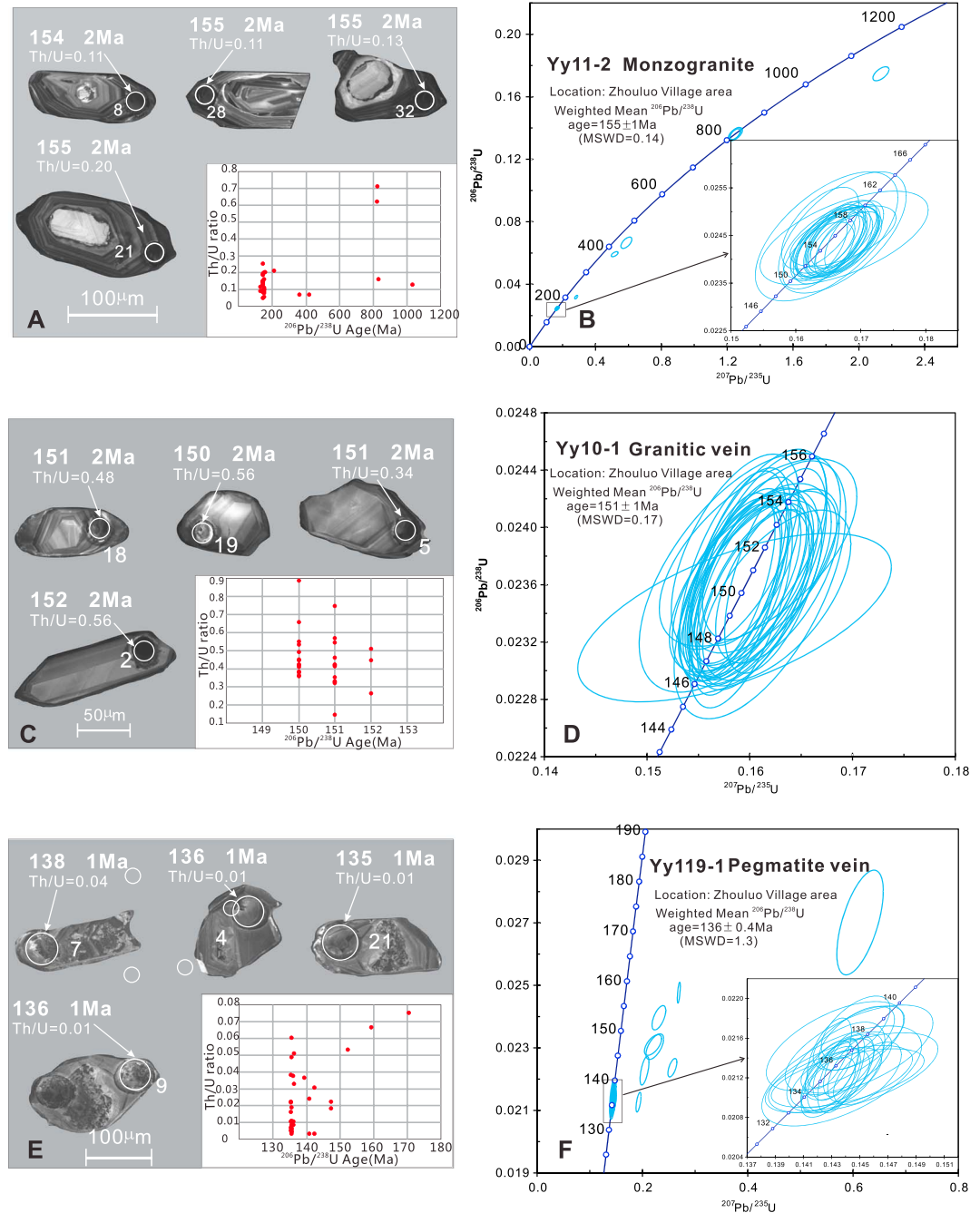


**Figure 14.** Cathodoluminescence (CL) images and LA-ICP-MS zircon dating results for rock samples from the Lianyungshan segment. MSWD, mean square of weighted deviates.

#### 4.4.1.3. Brittle Normal Faults

The low-angle Hengshan detachment fault bounds the folded domains to the NW (Figure 12a). This gently, NW dipping fault (Figure 13h) extends ~150 km in NE-SW direction across the southern and central parts of the Jiangnan Orogen (Figure 1) and bears dip-slip striations that record NW-SE extension [Li *et al.*, 2013]. The immediate footwall of the detachment is characterized by ~2 m thick gouges and mineralized breccias formed during brittle reworking of the metamorphic rocks, in agreement with the brittle definition for the detachment of Li *et al.* [2013]. Recent structural and thermochronological data illustrate that the detachment accommodated ~8–12 km of slip at rates of 0.14–1 mm/yr between 136 and 80 Ma [Li *et al.*, 2015a].

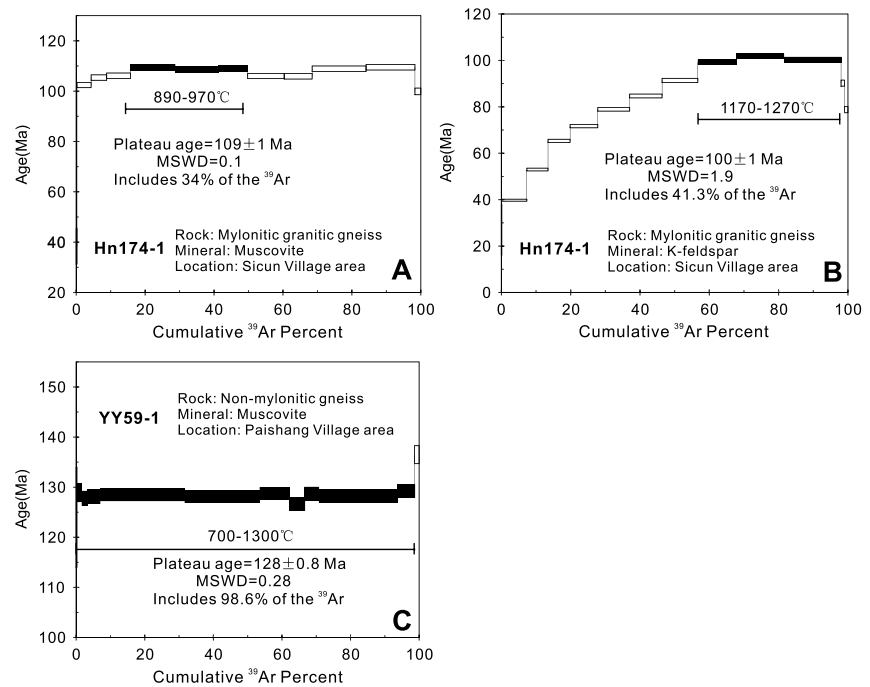


**Figure 15.** Biotite and muscovite  $^{40}\text{Ar}/^{39}\text{Ar}$  data for mylonitic gneisses from the Lianyunshan segment.

The hanging wall of the detachment fault is occupied by a supradetachment Cretaceous basin filled with red lacustrine sedimentary rocks (Figure 12a) that are cut by arrays of moderately to steeply dipping normal faults (Figure 13i). The faults strike NE-SW and contain brittle NW-SE striations associated with down-dip-slip criteria, kinematically consistent with normal faulting induced by NW-SE extension (Figure 12f). Their generation, genetically compatible with the extensional fabrics from the Hengshan dome located  $\sim 100$  km southwest of our study area [Li *et al.*, 2013], indicates that the Lianyunshan domain of the central Jiangnan Orogen underwent significant NW-SE extension in Cretaceous time.

#### 4.4.2. Zircon U-Pb Geochronology

Three samples were dated using zircon U-Pb geochronology to constrain the time of tectonism and magmatism in the Lianyunshan area.

Sample Yy11-2 is an undeformed, cross-cutting monzogranite emplaced at the easternmost end of zone 1 (Figure 13j). Zircon grains from this sample show dark and bright luminescent cores surrounded by thick sector-zoned rims under CL (Figure 14a) and have nearly consistent Th/U ratios of 0.1–0.2 apart from two inherited cores (Figure 14a and Table S2). Twenty-five concordant analyses of the oscillatory-zoned overgrowths yield a weighted mean  $^{206}\text{Pb}/^{238}\text{U}$  age of  $155 \pm 1$  Ma (MSWD=0.14) (Figure 14b), here interpreted as the crystallization age of the monzogranite. Seven cores yield greatly discordant ages ranging from 202 to 1396 Ma (Table S2) that are interpreted as the inheritance from adjacent gneiss and granitoids.

Sample Yy10-1 is a granitic melt that intruded along the folded schistosity within the gneisses (Figure 13k). Zircon grains from this sample show consistent, euhedral, and concentric zoned textures under CL and have high Th/U ratios of 0.2–0.9 (Figure 14c and Table S2). Thirty-two concordant analyses yield a weighted mean  $^{206}\text{Pb}/^{238}\text{U}$  age of  $151 \pm 1$  Ma (MSWD=0.17) (Figure 14d), herein interpreted as the crystallization age of the granitic vein. On the basis of its consistent age with sample Yy11-2, we assumed that the two samples were derived from the same magmatic source responsible for the generation of the Lianyunshan granitoids.

Sample Yy119-1 is an undeformed pegmatite vein that highly cuts across the foliated granitoids and mylonitic leucosomes (Figure 13f). Zircon grains from this sample display dark luminescent and faintly oscillatory-zoned textures under CL (Figure 14e) and have low Th/U ratios ( $<0.1$ ) due to high U contents (Table S2). Twenty-four concordant analyses yield a weight mean  $^{206}\text{Pb}/^{238}\text{U}$  age of  $136 \pm 0.4$  Ma (MSWD=1.3) (Figure 14f), which we interpreted as the crystallization age of the pegmatite vein. Other eight discordant analyses yield ages in the range of 147–172 Ma (Figure 14f) that possibly reflect the inheritance from the surrounding rocks.

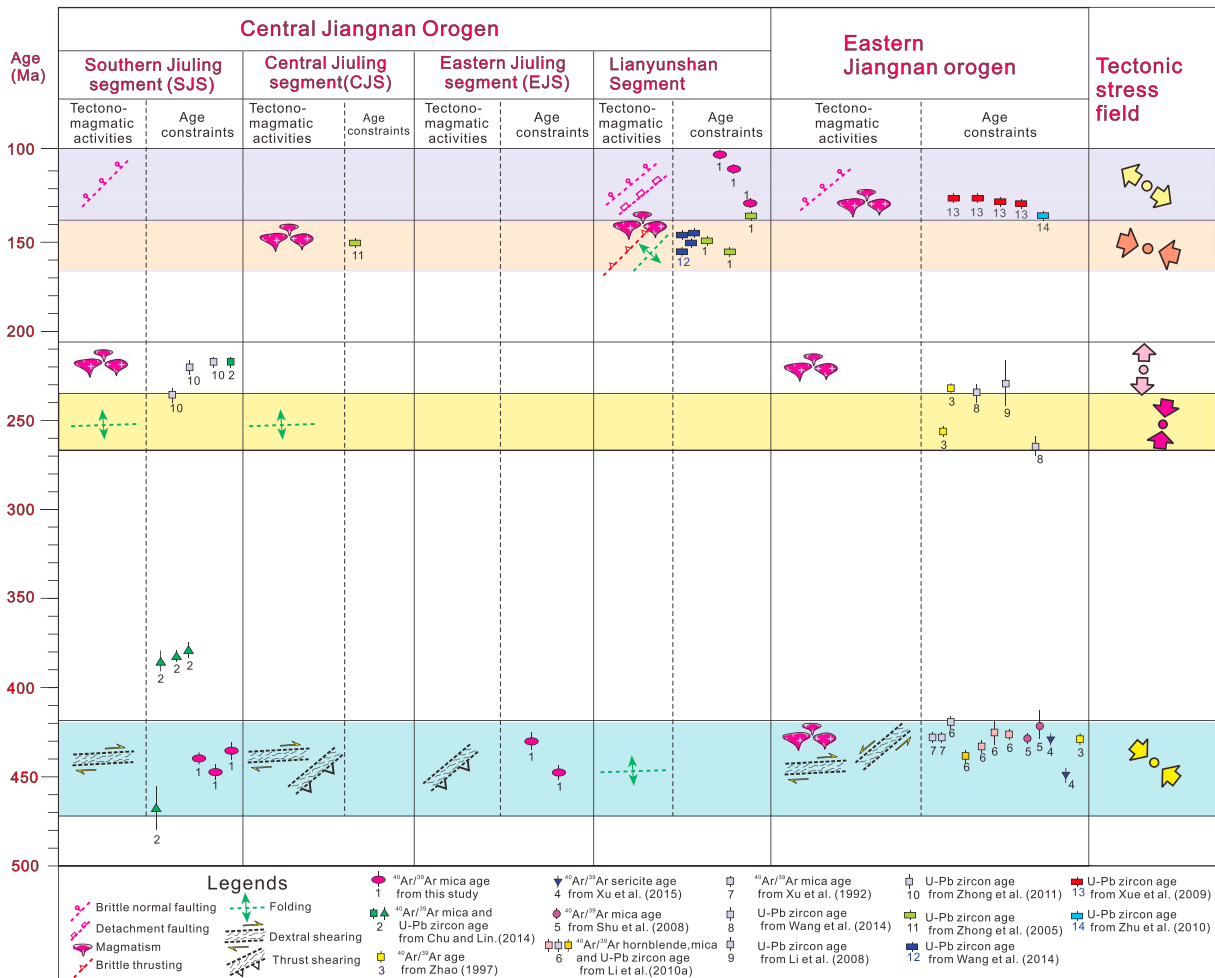


Figure 16. Time-space plot of the compiled geochronological and thermochronological data from across the Central and Eastern Jiangnan Orogens.

#### 4.4.3. $^{40}\text{Ar}/^{39}\text{Ar}$ Thermochronology

Sample Hn174-1 is a mylonitic granitic gneiss from zone 1 that exhibits a steeply south dipping foliation and a gently west plunging lineation associated with sinistral shearing. Mica-fish-shaped muscovites yield a plateau at  $109 \pm 1$  Ma covering 34% of the total  $^{39}\text{Ar}$  (Figure 15a) and a consistent isochron age of  $108 \pm 1$  Ma (MSWD = 0.46) with a near-atmospheric initial  $^{40}\text{Ar}/^{36}\text{Ar}$  value ( $376 \pm 54$ ) (Table S1). The coexisting K-feldspars yield a climbing age spectrum, from ages of 40 Ma up to a flat plateau at  $100 \pm 1$  Ma covering 41.3% of the total  $^{39}\text{Ar}$  (Figure 15b). The younger K-feldspar and older muscovite apparent ages coincide well with theoretical systematics for a steadily exhumed system, indicating that this sample underwent monotonous cooling without being subjected to reburial or reheating during exhumation.

Sample YY59-1 is a nonmylonitic gneiss with a folded schistosity that was collected from the ~E trending fold zone (see Figure 12a for its location). Muscovites therein yield a well-defined plateau at  $128 \pm 0.8$  Ma including 12 steps (Steps 1–12) and 98.6%  $^{39}\text{Ar}$  (Figure 15c and Table S2) and an identical isochron age of  $128 \pm 1$  Ma (MSWD = 1.07) with a near-atmospheric initial  $^{40}\text{Ar}/^{36}\text{Ar}$  value ( $297 \pm 4$ ).

### 5. Discussion

Our structural, geochronological, and thermochronological data, coupled with previous work, enable the establishment of a time-space plot (Figure 16) that summarizes the absolute time framework of observed structural fabrics from the Jiuling and Lianyunshan segments. The discussion below presents first the time estimates on major structures of each segment, second the Phanerozoic kinematic evolution of the

Jiangnan Orogen inferred from time-constrained sequential structural events, and finally their geodynamic origins and tectonic implications.

## 5.1. Time Estimates on Major Structures of the Four Segments

### 5.1.1. The Southern Jiuling Segment

Dextral shearing at temperatures of 400–500°C along the Baishui shear zone predates cooling below ~400°C at 447–439 Ma as constrained by our muscovite and biotite  $^{40}\text{Ar}/^{39}\text{Ar}$  cooling ages. Previous  $^{40}\text{Ar}/^{39}\text{Ar}$  ages of ~382–386 Ma on biotite and ~460 Ma on muscovite from samples collected in and to the north of the Baishui shear zone led *Chu and Lin* [2014] to relate the dextral shearing to an early Paleozoic orogenic event within south China. They interpreted the ~460 Ma muscovite age as the age of deformation, the ~380 age determinations as recording the end of orogenesis and, based on U-Pb ages of the metamorphic zircons, placed the initiation of orogenesis at ~465 Ma [*Z. X. Li et al.*, 2010]. We agree, except that we place the termination of orogenesis at ~420 Ma (Figure 16), on the basis of (1) the regional unconformity at the base of the Lower Devonian conglomerate [e.g., *Shu et al.*, 2014] and (2) widespread ~450–420 Ma S-type and adakitic intrusions interpreted as synorogenic crustal melts [e.g., *Wang et al.*, 2011, 2013a; *Li et al.*, 2015b].

The widespread distribution of ENE striking folds and thrusts testifies to significant ~NNW-SSE contraction. Despite their regional importance, we have no firm constraint on the age of these structures. They may represent long-lived, composite structural features resulting from multiphase contractional deformation. Tight to isoclinal folds, traditionally related to the Yangtze-Cathaysia assembly [e.g., *X. L. Wang et al.*, 2007], involve the 860–820 Ma Shuangqiaoshan Group [*Wang et al.*, 2008] and are unconformably overlain by the flat-lying Xiushui Group (~820 Ma) [e.g., *Wang et al.*, 2013b], indicating a pre-820 Ma age of the earliest folding. The most recent folding about an ENE oriented axis occurred in middle Triassic time, based on (1) ENE striking folds at the southern margin of the Jiangnan Orogen involving Middle Triassic strata [*Wang et al.*, 2013a; *Chu and Lin*, 2014] and (2) U-Pb zircon ages of ~220 Ma on the undeformed Mengshan monzogranite (Figure 16), which intrudes and cuts ENE striking folds, providing an upper age limit on folding [e.g., *Zhong et al.*, 2011; *Chu and Lin*, 2014].

### 5.1.2. The Eastern Jiuling Segment

Our  $^{40}\text{Ar}/^{39}\text{Ar}$  cooling ages indicate that (1) zone 1 cooled below the muscovite closure temperature (~450–350°C) by  $431 \pm 4$  Ma and (2) zone 4 cooled below the biotite closure temperature (~350–250°C) by  $449 \pm 4$  Ma. Because deformation occurred at temperatures of 350–450°C, the cooling ages may record a late stage of ductile shearing. Therefore, we infer that the oblique thrust shearing in the EJS initiated prior to 449 Ma and continued until 431 Ma.

### 5.1.3. The Central Jiuling Segment

The dextral fabrics in the CJS are similar in geometric style and metamorphic conditions with those in the SJS, allowing the possibility of coeval deformation that requires the dextral CJS fabrics to have developed at ~460–420 Ma. Top-to-the-NW thrust shear fabrics in the CJS are comparable to those in the EJS. If correlative, the CJS thrust shearing is likely coeval with that in the EJS, at ~449–431 Ma.

### 5.1.4. The Lianyunshan Segment

The prominent pre-Devonian folds are similar to those in the SJS. Consistent with the aforementioned interpretation, the folds are considered as the cumulative product of multiple contraction events spanning from the Neoproterozoic to the middle Devonian.

The NE striking thrust faults and related folds may have formed in Late Jurassic time, as indicated by two main regional considerations: (1) these structures, involving Early to Middle Jurassic strata, are unconformably overlain by gently folded Cretaceous strata [*J. H. Li et al.*, 2012, 2014a, 2014b] and (2) the folds are intruded by undeformed granitoids that yield U-Pb zircon crystallization ages of 160–155 Ma [*Xu et al.*, 2009; *Y. Li et al.*, 2015].

The east striking sinistral shear zones are intruded by and predate the 155–150 Ma Lianyunshan granitoids.  $^{40}\text{Ar}/^{39}\text{Ar}$  ages of 109–100 Ma obtained from zone 1 are too young to be related to the sinistral shearing, but rather to record accelerated footwall exhumation during normal slip along the Hengshan detachment fault. Similarly, the  $^{40}\text{Ar}/^{39}\text{Ar}$  age of sample Yy59-1 also records a reheating and reequilibration of footwall fold zones at ~128 Ma during extension. The 128–100 Ma age range is narrower than the total duration of extensional deformation, as the above  $^{40}\text{Ar}/^{39}\text{Ar}$  ages only record a portion of the cooling process. Pegmatites that crystallized at ~136 Ma (sample Yy119-1) are inferred to be crustal melts produced during

extension and provide limit for the timing of the onset of extensional deformation. This speculation coincides well with previous work, in which *Li et al.* [2013] reported a similar age of  $136 \pm 1$  Ma from synkinematic albite fluid sampled in the Hengshan dome that was interpreted to mark the beginning of extension. Recent apatite fission track data demonstrate that normal motion on the Hengshan detachment fault continued until 80 Ma [*Li et al.*, 2015a].

## 5.2. Phanerozoic Kinematic Evolution of the Jiuling and Lianyunshan Domains of the Central Jiangnan Orogen, Regional Comparisons, and Their Geodynamic Implications

Synthesis of new data from this study with previous work concerning many of the other structures enables us to invoke plausible interpretations delineating Phanerozoic evolution of the Jiuling and Lianyunshan domains of the central Jiangnan Orogen. As a result, we propose a four-stage tectonic history (Figure 16) that explains the geodynamic relationships between episodic intraplate deformation and the evolving plate dynamics along boundaries of south China.

### 5.2.1. The Early Paleozoic NW-SE Crustal Contraction, Regional Comparisons, and Their Association With the Yangtze-Cathaysia Convergence

The early Paleozoic deformation in the Jiuling domain of the central Jiangnan Orogen was characterized by combined ductile dextral and thrust shearing that was variably partitioned into arrays of anastomosing high-strain zones. Dextral arrays characterize the SJS and CJS, which strike dominantly E-ESE and dip steeply to the south (Figure 16). Kinematically compatible and coeval thrust shear zones prevailed in the EJS and CJS, which strike NE, dip  $20\text{--}80^\circ$  to the SE and bear top-to-the-NW shear criteria (Figure 16). Together, these dextral and thrust shear zones operated as complementary structures accommodating regional NW-SE contraction during the early Paleozoic (460–420 Ma) in the Jiuling domain of the central Jiangnan Orogen (Figure 17a). To the east, the contraction locally reactivated the Neoproterozoic east striking zones in the eastern Jiangnan Orogen and resulted in significant dextral ductile shearing along the zones [*Xu et al.*, 2015].

In addition to the Jiangnan Orogen, the early Paleozoic NW-SE contraction also led to ubiquitous folding and ductile shearing in the north Cathaysia (Figure 17a). Specific deformation and metamorphism include (1) northwest verging folding and metamorphism in the Chencai Complex, along the Shaoxing-Jiangshan fault zone, occurred at lower crustal conditions ( $>8$  kbar and  $>800^\circ\text{C}$ ) between 460 and 440 Ma and was followed by exhumation or cooling to midcrustal conditions ( $<5$  kbar and  $<500\text{--}300^\circ\text{C}$ ) by 420 Ma [*Z. X. Li et al.*, 2010]; (2) pervasive NW-SE shortening throughout the Wuyishan of north Cathaysia at 453–433 Ma, recorded by synkinematic monazites [*Faure et al.*, 2009; *Charvet et al.*, 2010]; and (3) northwest verging ductile thrust shearing along the northern margin of the Wuyishan at 432–421 Ma as constrained by biotite and muscovite  $^{40}\text{Ar}/^{39}\text{Ar}$  ages [*Shu*, 2006; *Shu et al.*, 1999, 2008a, 2008b, 2015], and a younger muscovite age of  $391 \pm 3$  Ma [*Shu et al.*, 1999], which may reflect cooling after southwestward sinistral shearing along the southern margin of the Wuyishan (*Li et al.*, under review, 2016). The above-stated deformation and metamorphism were accompanied by voluminous 460–420 Ma magmatism, crustal melting, and migmatization in the Cathaysia Block and the Jiangnan Orogen [*Y. J. Wang et al.*, 2007, 2011, 2013a, and references therein] (Figure 17a). These geological features, taken together, suggest considerable tectonic reorganization during orogenic contraction in early Paleozoic time. In this tectonic scenario, the shear zones developed primarily along preexisting lithological and structural contacts, suggesting that inherited structures effectively localized strain at elevated temperatures and pressures.

Early Paleozoic tectonism can be interpreted as an intracontinental orogenic event resulting from continued convergence between the previously amalgamated Yangtze and Cathaysia Blocks [e.g., *Charvet et al.*, 2010; *Z. X. Li et al.*, 2010; *Faure et al.*, 2009; *Shu et al.*, 2015; *Song et al.*, 2015]. However, two significant observations remain poorly explained: (1) the southeast Yangtze exhibits much less Paleozoic deformation and metamorphism in comparison to either the Jiangnan Orogen or the north Cathaysia and (2) the highest grade metamorphic rocks, characterized by amphibolite facies metamorphism and clockwise P-T paths, are rare and mostly limited to the preexisting Shaoxing-Jiangshan suture zone [*Z. X. Li et al.*, 2010; *Wang et al.*, 2016].

By integrating the spatial distribution of synorogenic deformation, metamorphism, and magmatism, an early Paleozoic orogen extending across the Jiangnan Orogen into the north Cathaysia can be traced (Figure 17a). The southern edge of the Jiangnan Orogen marks the core zone along which early Paleozoic Yangtze-Cathaysia convergence was accommodated (Figure 17b). To the northwest, convergence in the southeast Yangtze was accommodated by the development of NW verging folds and thrusts, which root to the SE into

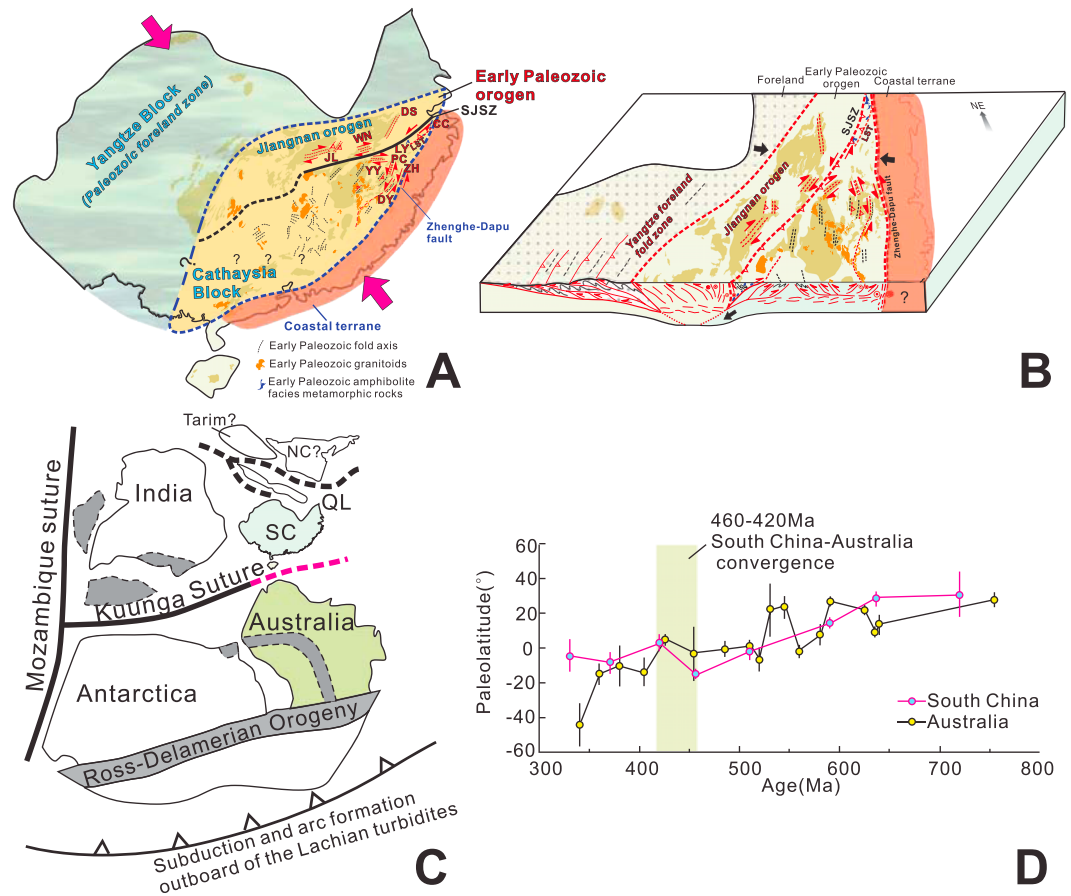


**Figure 17.** (a) Available data on early Paleozoic tectonism and magmatism in south China, which aid in tracing an early Paleozoic orogen extending through the Jiangnan Orogen into the north Cathaysia Block. The orogen is separated from a coastal terrane preserving distinctly different Paleoproterozoic basement and Triassic metamorphism by the Zhenghe-Dapu fault. Abbreviations: ZH, Zhenghe shear zones (Li et al., under review, 2016); PC, Pucheng shear zones (Li et al., under review, 2016); CC, Chencai shear zones (Li et al., under review, 2016); DY, Dongyou shear zones (Li et al., under review, 2016); YY, Yiyang shear zones [Shu et al., 2015]; JL, Jiuling shear zones (this study); WN, Wannian shear zones [Xu et al., 1992]; DS, Dexing and Shexian shear zones [Xu et al., 2015]; LY, Longyong amphibolite facies metamorphic rocks [Wang et al., 2016]; LST, Luodian-Sanjie Thrust (Li et al., under review, 2016); (b) Craton figure shows a Yangtze-Cathaysia intraplate convergence model to explain the early Paleozoic deformation in south China. The southern edge of the Jiangnan Orogen marks the core of the convergence, characterized by combined dextral and thrust ductile shearing that was variably partitioned in arrays of anastomosing high-strain zones. To its northwest, structural styles in the southeast Yangtze support to interpret it as a foreland fold-and-thrust zone during convergence. To its southeast, the convergence exerted a compressional force that caused extensive ductile shearing, folding, and metamorphism in the Cathaysia Block. (c) Simplified reconstruction of Gondwana showing the location of south China and the Kuunga Suture marking final amalgamation of south China and Australia (modified after Boger et al. [2001], Xu et al. [2014a, 2014b], Metcalfe [2013], Ali et al. [2013], Kusky et al. [2003], and Meert [2003]). (d) Comparison of paleolatitudes for south China and Australia from the Neoproterozoic to the early Paleozoic, according to recent paleomagnetic data from Han et al. [2015].

a basal décollement beneath the Jiangnan Orogen, manifesting northwest directed propagation deformation and supporting interpretation of the southeast Yangtze as a foreland fold and thrust zone during convergence (Figure 17b). To the south, the Shaoxing-Jiangshan suture zone might have acted as a weak inherited structural discontinuity and enough weakness, along which reactivation facilitated burial by northwestward underthrusting that gave rise to the observed high-pressure (>8 kba) metamorphic assemblages [Z. X. Li et al., 2010]. Subsequent southeastward thrusting and northwestward back thrusting might have operated interactively and together brought the high-grade ductily metamorphic rocks [e.g., Wang et al., 2016] to the surface (Figure 17b). In the Cathaysia area, convergence caused folding, thrusting and metamorphism, and strain localization along preexisting NE striking structures generated arrays of thrust and sinistral ductile shear zones (Figure 17b) [Shu, 2006, Shu et al., 2015; Charvet et al., 2010; Faure et al., 2009; Li et al., under review, 2016]. The Zhenghe-Dapu fault forms the eastern boundary of the early Paleozoic orogen. East of this

fault is a coastal terrane that preserves a distinctly different Paleoproterozoic basement overprinted by Triassic metamorphism (Figure 17a) [Yin, 2014; Zhao, 2015]. The nature of this terrane and the timing of its accretion to the orogen remain undetermined.

Another question concerns what was the external force to drive the early Paleozoic intraplate Yangtze-Cathaysia convergence. Deformation, metamorphism, and magmatism from the southeast Yangtze to the north Cathaysia show a broadly northwestward weakening trend, implying that the driving force for tectonism lay to the southeast. Lines of evidence from geochemistry, provenance, and paleomagnetism support that south China occupied a position between India, Antarctica, and Australia, along the northern margin of Gondwana during the Paleozoic (Figure 17c) [e.g., Cawood *et al.*, 2013; Yang *et al.*, 2004; Han *et al.*, 2015]. U-Pb and Hf isotope analyses of detrital zircons from the Hainan Island, combined with Ordovician arc magmatism in the Tuncang area [Xu *et al.*, 2007, 2008] and the Cambro-Ordovician unconformity in the Sanya area [Xu *et al.*, 2014a, 2014b], are consistent with the amalgamation of south China and Australia along its southernmost margin in the Ordovician [Xu *et al.*, 2014b]. Recent paleomagnetic data [Han *et al.*, 2015] show a gradual approach of the paleolatitudes of south China and Australia during the period 460–420 Ma (Figure 17d), implying that their final suturing might have not been accomplished until the middle Silurian. The Paleozoic Kuunga Suture may mark the collision zone along which Gondwana was finally assembled (Figure 17c) [Xu *et al.*, 2014b]. Therefore, the Paleozoic intraplate Yangtze-Cathaysia convergence may be a far-field consequence of such suturing.

### 5.2.2. The Middle Triassic ~NNE-SSW Contraction, Regional Comparisons, and Their Association With Continental Collision of South China With North China and the Indochina Block

In the Jiuling and Lianyunshan domains of the central Jiangnan Orogen, Middle Triassic ~NNE-SSW contraction has been recorded by E to ENE trending fold trains (Figures 16 and 18a) and thin-skinned north and south verging brittle thrusts [Chu and Lin, 2014]. Coevally, toward the south, the contraction was responsible for widespread E and ENE trending folds and a remarkable Late Triassic unconformity in the Cathaysia area [e.g., Zhang *et al.*, 2008; Wang *et al.*, 2013a; Shi *et al.*, 2015] (Figure 18a). In addition, NE trending dominantly ductile shear zones are localized along preexisting weaknesses and faults and yield  $^{40}\text{Ar}/^{39}\text{Ar}$  age determinations of 245–220 Ma. Examples include 239–230 Ma for the Changting dextral shear zone in the Wuyishan [Xu *et al.*, 2011], 248–220 Ma for the Wuchuan and Fengshan strike-slip shear zones [Wang *et al.*, 2007c], 213–195 Ma for the Hefu dextral shear zone in the Yunkai terrane [Zhang and Cai, 2009], 229–227 Ma for the Gezhen strike-slip shear zone in the Hainan Island [Chen *et al.*, 2006], 232–234 Ma for the Jiangshan-Xinyu strike-slip shear zone in the southern Jiangnan Orogen [Shu *et al.*, 2015], and 245–228 Ma for the Badu dextral shear zone in the Badu complex (Li *et al.*, under review, 2016) (Figure 18a). The above-stated thrust-and-fold and strike-slip structures are considered to be kinematically coupled, with contractile structures forming within restraining bends in an evolving strike-slip system [e.g., Sylvester, 1988; Cunningham and Mann, 2007]. We show that NE trending dextral ductile shear zones form transcurrent fault zones (lateral ramps) that link segments of ~E trending folds and thrusts (Figure 18b). As the strike-slip faulting kept transferring some of the oblique displacements into dip-slip thrusting and folding within adjacent regions, two paired restraining bends developed by imbricate contractional fans would be reasonably generated along two sides of the dextral shear zone (Figure 18b).

Two contrasting geodynamic interpretations have been proposed for Middle Triassic crustal thickening in south China: (1) flat-slab subduction of the Paleo-Pacific plate [Li and Li, 2007] and (2) continental collision of south China with Indochina and/or North China [Zhang and Cai, 2009; Xu *et al.*, 2011; Wang *et al.*, 2013a; Shu *et al.*, 2015]. The flat-slab model, based on the recognition of northwestward younging trends of Triassic thrusting, metamorphism, and synorogenic magmatism, is proposed to explain the development of a broad (~1300 km wide) NE trending fold-and-thrust belt [Li and Li, 2007]. There are arguments against the flat-slab model. Wang *et al.* [2013a], based on a detailed synthesis of geochronological data, have called into question the presence of temporal and spatial trends of magma used in support of the flat-slab model. The lack of an upper plate magmatic arc argues against the Paleo-Pacific subduction. Li *et al.* [2011] interpreted a 280–260 Ma set of plutons as a magmatic arc; however, there are no geochemical data to support this contention [Wang *et al.*, 2013a]. Finally, some NE trending folds and thrusts involve Middle Jurassic sandstones, implying a post-Middle Jurassic rather than Middle Triassic age for deformation [Zhang *et al.*, 2008].

We interpret the Triassic ~NNE-SSW contraction of south China as a consequence of continental collision (Figure 18c). In this tectonic scenario, the Paleo-Tethyan Ocean closed diachronously from west to east beginning in the late Early Permian [Yin and Nie, 1993, 1996]. The diachroneity resulted from an ~70° clockwise rotation and northward penetration of south China relative to North China [Zhao and Coe, 1987;

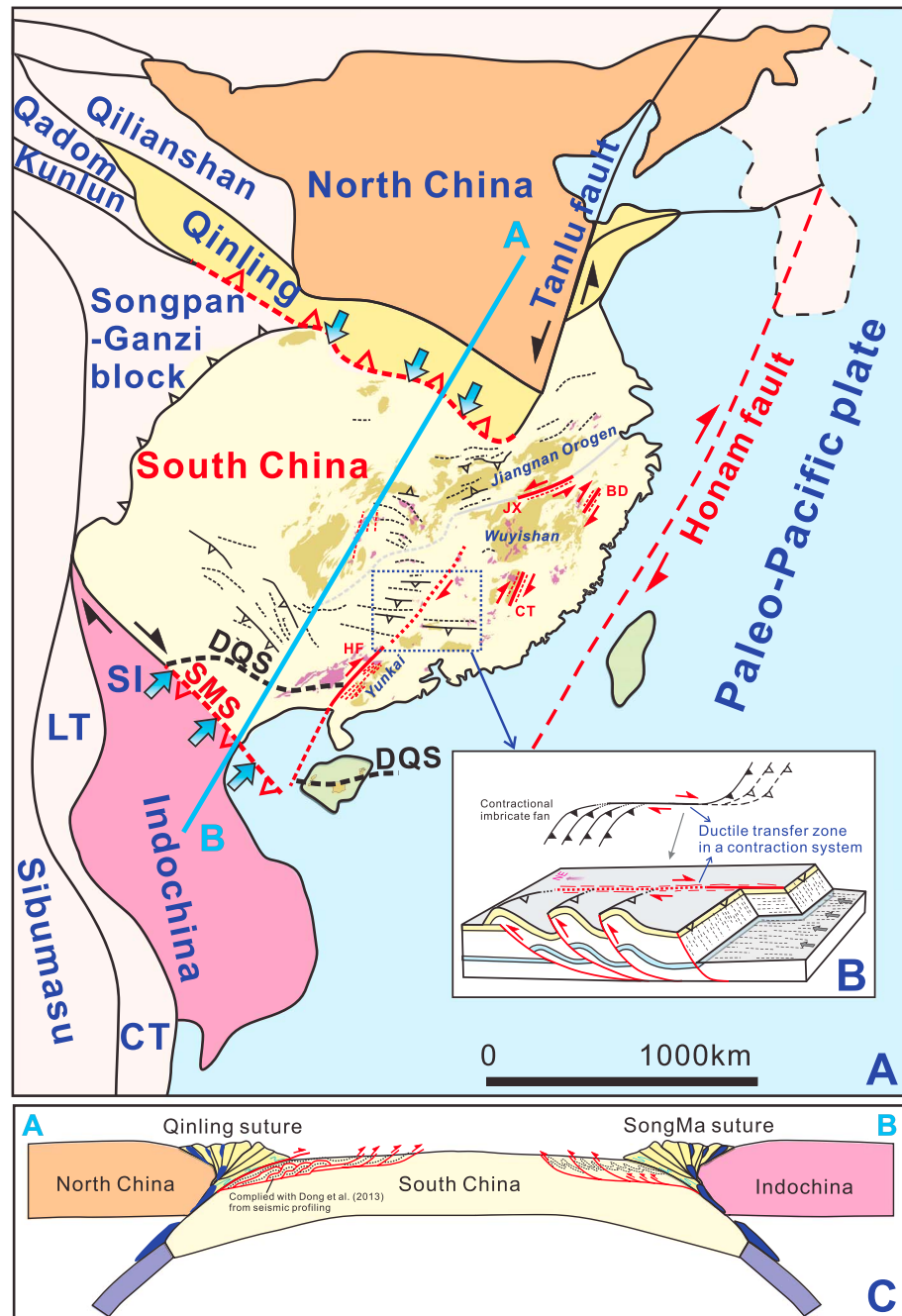


**Figure 18.** (a) Simplified geological map showing the Triassic structures and magmatic rocks in south China and adjacent regions. HF, the Hepu shear zone; CT, the Changting shear zone; BD, the Badu shear zone; JX, the Jiangshan-Xinyu shear zone. (b) A structural model to explain the kinematic coupling between the thrust-and-fold and strike-slip structures, in which strike-slip faulting keeps transferring some of the oblique displacements into adjacent regions that generates paired restraining bends of imbricate thrusts and folds. (c) A sketch showing the continental collisions of south China with North China and Indochina during the Middle Triassic.

Enkin et al., 1992]. The south China “indenter” penetrated between the North China and the Indochina Blocks along its northern and southern margins, respectively (Figure 18c) [Li, 1994; Lin, 1995; Hacker et al., 1998; Carter et al., 2001; Zhang et al., 2001; Lepvrier et al., 2004; Dong et al., 2011; Faure et al., 2014; Li et al., 2015c; Halpin et al., 2015]. Intraplate deformation within the south China indenter was partitioned between prevailing NNE-SSW transpressional structures and NE striking right-lateral strike-slip transcurrent shear zones (Figure 18a).

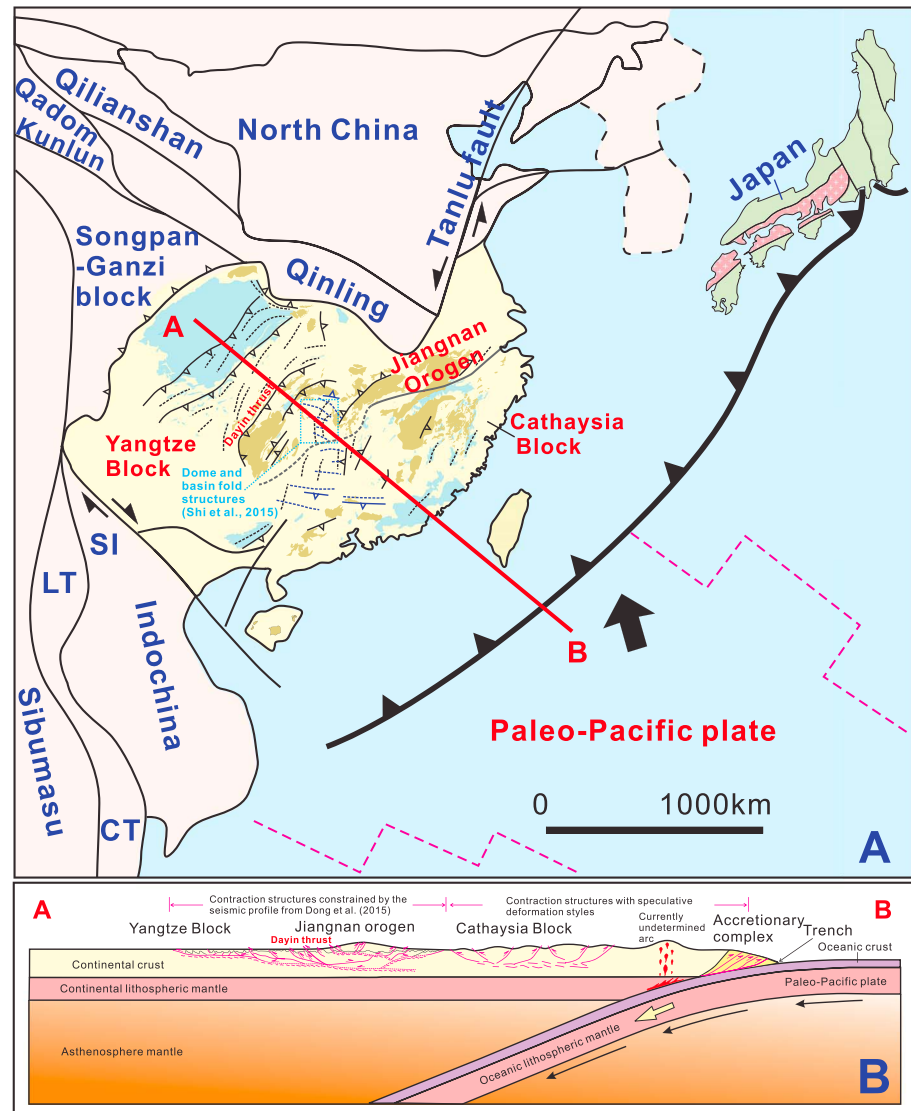


**Figure 19.** (a) Simplified geological map showing the Late Jurassic structures in south China. (b) A sketch showing a subduction-related model to interpret the Late Jurassic evolution of south China, in which the pronounced NE trending folds and thrusts are related to northwestward subduction of the Paleo-Pacific plate.

**5.2.3. The Late Jurassic NW-SE Contraction, Regional Comparisons, and Their Association With the Subduction of the Paleo-Pacific Plate**

Late Jurassic NE trending thrusts and fault-related folds, mainly localized in the Lianyunshan segment, record a younger NW-SE contraction (Figure 16). Similar structures are well developed throughout the Yangtze and Cathaysia areas. In the Yangtze area, thin- and thick-skinned thrust sheets separated by the Dayin thrust [Yan et al., 2003] (Figure 19a) have accommodated 160 km of shortening [Mei et al., 2010; Li et al., 2014a] via in- and out-of-sequence thrusting above several detachment layers [Yan et al., 2009]. In the Cathaysia area, map-scale NE trending anticlinoriums that overprint Triassic ~E trending anticlinoriums has created a dome and basin interference pattern with wavelengths of tens of kilometers (Figure 19a) [Zhang et al., 2008; Shi et al., 2015]. The duration of this contractional event remains poorly constrained. Based on regional considerations, the youngest strata involved in contractional deformation are the Middle Jurassic [Zhang et al., 2008; Li et al., 2014a], indicating that this contraction event initiated during or soon after the deposition of Middle Jurassic strata. Notably, voluminous rhyolitic and basaltic magma erupted at ~190–165 Ma, forming an ~40 km wide E-W trending bimodal volcanic zone that extends for >250 km in the Nanling Range of central Cathaysia [Deng et al., 2004; Zhou et al., 2005; Xu et al., 2009; Shu et al., 2009]. This magmatism implies a rifting setting

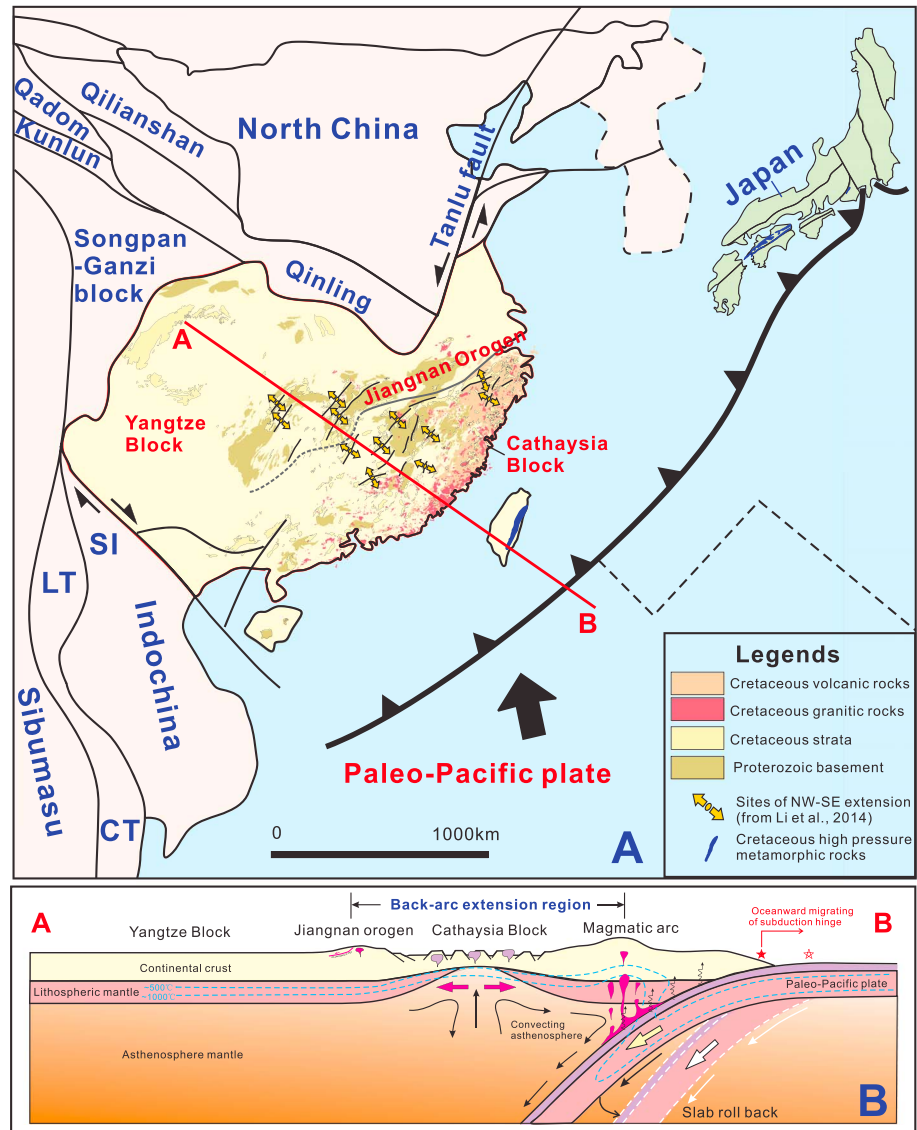


**Figure 20.** (a) Simplified geological map showing the Cretaceous structures and magmatic rocks in south China. Early Cretaceous (~100 Ma) high-pressure metamorphic rocks in SW Japan might have been produced by the collision between the Philippine block and the Japanese arc [Minato and Hunahashi, 1985; Ichikawa et al., 1990]. (b) The cartoon figure shows the back-arc extension model to explain the widespread Cretaceous extensional structures and magmatic rocks in south China. The back-arc extension was associated with roll-back or retreat of the subducting Paleo-Pacific plate.

in the Early to Middle Jurassic. Accordingly, the contractional event most likely commenced in Late Jurassic time and postdated the Early to Middle Jurassic continental rifting.

Geodynamically, the leading model for driving intraplate contractional deformation and orogeny is oceanic subduction, whereby stress coupling of a downgoing oceanic plate to the upper plate transmitted stresses inlandward, producing a broad intraplate orogen featuring extensive fold-and-thrust belt and décollement generation but with less magmatic arc development [e.g., English et al., 2003; English and Johnston, 2004]. For example, the Laramide orogeny, creating the broad Rocky Mountain fold-and-thrust belt in Canada and the United States which developed >700 km inboard of the nearest convergent margin, was interpreted as resulting from the flat-slab subduction in response to the subduction of (1) the Kula-Farallon spreading center or (2) a buoyant oceanic plateau [Livaccari et al., 1981; Bird, 1988; Murphy et al., 2003]. Similarly, the intraplate deformation in Andes formed as a tectonic response to subduction, whereby the inland east migrating, thin-skinned thrust belt located 700–800 km from the trench resulted from the subduction of

the Nazca plate [Jordan *et al.*, 1983]. For the south China case, the Late Jurassic structures record NW-SE compression consistent with coeval northwestward subduction of the Paleo-Pacific plate [Maruyama, 1997], and we therefore concur with many authors [e.g., Lin *et al.*, 2008; Zhang *et al.*, 2008; Wang *et al.*, 2013a], in explaining the contraction as a consequence of the Paleo-Pacific plate subduction beneath south China (Figure 19b).

#### 5.2.4. The Cretaceous NW-SE Extension, Regional Comparisons, and Their Association With Roll-Back of the Subducting Paleo-Pacific Plate

Cretaceous NW-SE extension is recorded by brittle normal faults and the low-angle Hengshan detachment fault in the Lianyunshan segment (Figure 16) and ductile shear zones at greater depth in the Hengshan dome [Li *et al.*, 2013]. Cretaceous cooling ages that characterize older sinistral shear zones and folds imply reactivation and reheating during extension. The extension and resultant exhumation may have facilitated footwall erosion that allowed the final exposure of the structurally lower shear zones and folds in the Lianyunshan segment.

There is growing evidence for Cretaceous crustal extension in the Cathaysia area. It has been demonstrated that rifting, subsidence, doming, and rapid exhumation were widespread and started simultaneously that recorded regional NW-SE extension [Lin *et al.*, 2000; Shu *et al.*, 2009; Wang and Shu, 2012; J. H. Li *et al.*, 2012, 2014b] (Figure 20a). Thermochronological studies constrain extension to 136–80 Ma [Li *et al.*, 2015a], coeval with 136 to 86 Ma extension-related magmatism [e.g., Zhou and Li, 2000; Li, 2000; Li *et al.*, 2014a]. The coeval extension and magmatism require a regional rather than local explanation. Roll-back of the subducting Paleo-Pacific plate (Figure 20b) could explain (1) parallelism of the extension direction and the direction of coeval Paleo-Pacific subduction [e.g., Engebretson *et al.*, 1985], (2) the geochemical arc-signatures of Cretaceous igneous rocks [e.g., Zhou and Li, 2000; Jiang *et al.*, 2011], (3) the oceanward younging of Cretaceous magmatism [Li *et al.*, 2014a], and (4) the oceanward decrease of  $T_{DM}^C$  and increase of  $\epsilon_{Nd(t)}$  in Cretaceous igneous rocks [Jahn *et al.*, 1976; Gilder *et al.*, 1996; Chen and Jahn, 1998].

## 6. Conclusions

We report here evidence for four stages of deformation in the Jiuling and Lianyunshan domains of the central Jiangnan Orogen. Their structural features and tectonic implications for understanding Phanerozoic tectonic evolution of south China are summarized below.

1. Early Paleozoic NW-SE contraction, dated at 460–420 Ma, gave rise to dextral and northwest directed thrust shearing, under greenschist-facies conditions (~400–500°C). This contraction, occurred synchronously with pervasive ductile shearing, metamorphism, and magmatism in the Cathaysia area, resulting from the continued Yangtze-Cathaysia convergence externally driven by the suturing of south China with Australia
2. Middle Triassic NNE-SSW contraction was accommodated by regional ~E-W folds and thrusts. This deformation stage, together with coeval dextral shearing along NE-SW shear zones in the Cathaysia area, is attributed to continental collision of south China with North China and Indochina.
3. Middle-Late Jurassic NW-SE contraction produced NE-SW thrusts and fault-related folds. The contraction is extensively documented in south China and interpreted as a consequence of northwestward subduction of the Paleo-Pacific plate.
4. Cretaceous NW-SE extension led to brittle normal faulting, basin opening, exhumation, and reheating in the Lianyunshan Segment. This extension, responsible for widespread development of magmas, basins, and dome structures, was associated with roll-back of the subducting Paleo-Pacific plate.

## References

- Ali, J. R., H. M. C. Cheung, J. C. Aitchison, and Y. Sun (2013), Palaeomagnetic re-investigation of Early Permian rift basalts from the Baoshan Block, SW China: Constraints on the site-of-origin of the Gondwana-derived eastern Cimmerian terranes, *Geophys. J. Int.*, *193*, 650–663.
- Andersen, T. (2002), Correction of common lead in U-Pb analyses that do not report  $^{204}\text{Pb}$ , *Chem. Geol.*, *192*, 59–79.
- Bird, P. (1988), Formation of the Rocky Mountains, western United States: A continuum computer model, *Science*, *239*, 1501–1507.
- Boger, S. D., C. J. L. Wilson, and C. M. Fanning (2001), Early Paleozoic tectonism within the East Antarctic craton: The final suture between east and west Gondwana?, *Geology*, *29*, 463–466.
- Carter, A., D. Roques, and C. Bristow (2001), Understanding Mesozoic accretion in southeast Asia: Significance of Triassic thermotectonism (Indosinian Orogen) in Vietnam, *Geology*, *29*(3), 211–214.
- Cawood, P. A., Y. J. Wang, Y. J. Xu, and G. C. Zhao (2013), Locating South China in Rodinia and Gondwana: A fragment of greater India lithosphere?, *Geology*, *41*, 903–906.
- Charvet, J. (2013), The Neoproterozoic-Early Paleozoic tectonic evolution of the South China Block: An overview, *J. Asian Earth Sci.*, *74*, 198–209.

### Acknowledgments

Data supporting this article are either included as supporting information or are available by contacting the corresponding author. This work was financially supported by a NSFC Project (41190075) entitled “Final Closure of the Paleo-Asian Ocean and Reconstruction of East Asian Blocks in Pangea,” which is the fifth research project of NSFC Major Program (41190070) “Reconstruction of East Asian Blocks in Pangea,” Hong Kong RGC GRF (HKU7063/13P and 17301915), and Natural Science Foundation of China (41502197) and Chinese Geological Survey Project (12120115069501). S.T. Johnston was supported by an NSERC Discovery Grant (RGPIN-2014-06533). We thank the Editor Paul Tregoning, and two reviewers J. Charvet and L. S. Shu for their critical, careful, and very constructive reviews that have helped improve the clarity and interpretations of the original draft. Helpful discussions with Yigui Han and Pengfei Li improved the manuscript. Jianhua’s work in Hong Kong has been supported by grants from Hong Kong Scholars Program.

- Charvet, J., L. S. Shu, Y. S. Shi, L. Z. Guo, and M. Faure (1996), The building of south China: Collision of Yangtze and Cathaysia blocks, problems and tentative answers, *J. Southeast Asian Earth Sci.*, *13*(3–5), 223–235.
- Charvet, J., D. Cluzel, M. Faure, M. Caridroit, L. S. Shu, and H. F. Lu (1999), Some tectonic aspects of the pre-Jurassic accretionary evolution of East Asia, in *Gondwana Dispersion and Asian Accretion, IGC321 Final Results Volume*, edited by I. Metcalfe et al., pp. 37–65, Balkema.
- Charvet, J., L. S. Shu, M. Faure, F. Choulet, B. Wang, H. F. Lu, and N. L. Breton (2010), Structural development of the Lower Paleozoic belt of South China: Genesis of an intracontinental orogen, *J. Asian Earth Sci.*, *39*, 309–330.
- Chen, A. (1999), Mirror thrusting in the south China Orogenic belt: Tectonic evidence from western Fujian, southeastern China, *Tectonophysics*, *305*, 497–519.
- Chen, J. F., and B. M. Jahn (1998), Crustal evolution of southeastern China: Nd and Sr isotopic evidence, *Tectonophysics*, *284*(1–2), 101–133.
- Chen, J. F., K. A. Foland, F. M. Xing, X. Xu, and T. X. Zhou (1991), Magmatism along the southeast margin of the Yangtze block: Precambrian collision of the Yangtze and Cathaysia blocks of China, *Geology*, *19*, 815–818.
- Chen, W., X. Y. Liu, and S. H. Zhang (2002), Continuous laser stepwise heating  $^{40}\text{Ar}$ - $^{39}\text{Ar}$  dating technique [in Chinese with English abstract], *Geogr. Rev.*, *48*(Suppl), 127–134.
- Chen, X. Y., Y. J. Wang, M. Wei, W. M. Fan, and T. P. Peng (2006), Microstructural characteristics of the NW-trending shear zones of Gongai region in Hainan Island and its  $^{40}\text{Ar}$ - $^{39}\text{Ar}$  geochronological constraints [in Chinese with English abstract], *Geotecton. Metallog.*, *30*(3), 312–319.
- Chen, X., J. Y. Rong, C. E. Mitchell, D. A. T. Happer, J. X. Fan, R. B. Zhan, Y. D. Zhang, R. Y. Li, and Y. Wang (2000), Late Ordovician to earliest Silurian graptolite and brachiopod zonation from Yangtze Region, South China with a global correlation, *Geol. Mag.*, *137*(6), 623–650.
- Chu, Y., and W. Lin (2014), Phanerozoic polyorogenic deformation in southern Jiuling massif, northern South China block: Constraints from structural analysis and geochronology, *J. Asian Earth Sci.*, *86*(1), 117–130.
- Chu, Y., W. Lin, M. Faure, Q. C. Wang, and W. B. Ji (2012), Phanerozoic tectonothermal events of the Xuefengshan Belt, central South China: Implications from U–Pb age and Lu–Hf determinations of granites, *Lithos*, *150*, 243–255.
- Cunningham, W. D., and P. Mann (2007), Tectonics of strike-slip restraining and releasing bends, *Geol. Soc. Lond., Spec. Publ.*, *290*, 1–12.
- Deng, P., L. S. Shu, X. Q. Yu, Y. Sun, B. Wang, and Z. Z. Tan (2004), Early-Middle Jurassic basins and features of volcanic rocks in the western Fujian-southern Jiangxi Region, *Acta Petrol. Sin.*, *20*(3), 521–532.
- Deprat, J. (1914), Etude des plissements et des zones décaissement de la moyenne et de la basse Rivièrè Noire, *Mem. Serv. Geol. Indochine*, *3*, 59.
- Ding, D. G., T. L. Guo, Y. L. Liu, and C. B. Zhai (2007), Structural attribute of the Jiangnan–Xuefengshan belt, China: A discussion [in Chinese with English abstract], *Geol. Bull. China*, *26*(7), 801–809.
- Dong, S. W., Y. Q. Zhang, R. Gao, J. B. Su, M. Liu, and J. H. Li (2015), A possible buried Paleoproterozoic collisional orogen beneath central South China: Evidence from seismic-reflection profiling, *Precambrian Res.*, *264*, 1–10.
- Dong, Y. P., G. W. Zhang, F. Neubauer, X. M. Liu, J. Genser, and C. Hauzenberger (2011), Tectonic evolution of the Qinling orogen, China: Review and synthesis, *J. Asian Earth Sci.*, *41*, 213–237.
- Engelbreton, D., A. Cox, and R. G. Gordon (1985), Relative plate motions between ocean and continental plates in the Pacific basin, *Geol. Soc. Am. Spec. Pap.*, *206*, 1–59.
- English, J. M., and S. T. Johnston (2004), The Laramide orogeny: What were the driving forces?, *Int. Geol. Rev.*, *46*, 833–838.
- English, J. M., S. T. Johnston, and K. L. Wang (2003), Thermal modeling of the Laramide orogeny: Testing the flat-slab subduction hypothesis, *Earth Planet. Sci. Lett.*, *214*, 619–632.
- Enkin, R. J., Z. Yang, Y. Chen, and V. Courtillot (1992), Paleomagnetic constraints on the geodynamic history of the major blocks of China from Permian to the present, *J. Geophys. Res.*, *97*, 13,953–13,989, doi:10.1029/92JB00648.
- Etchecopar, A., and G. Vasseur (1987), A 3-D kinematic model of fabric development in polycrystalline aggregates: Comparisons with experimental and natural examples, *J. Struct. Geol.*, *9*(5–6), 705–717.
- Faure, M., L. S. Shu, B. Wang, J. Charvet, F. Choulet, and P. Monié (2009), Intracontinental subduction: A possible mechanism for the Early Paleozoic Orogen of SE China, *Terra Nova*, doi:10.1111/j.1365-3121.2009.00888.
- Faure, M., C. Lepvrier, V. V. Nguyen, T. V. Vu, W. Lin, and Z. C. Chen (2014), The South China block-Indochina collision: Where, when, and how?, *J. Asian Earth Sci.*, *79*, 260–274.
- Fromaget, J. (1932), Sur la structure des Indosinides, *C. R. Hebd. Seances Acad. Sci.*, *195*, 538.
- Gao, L. Z., J. Chen, X. Z. Ding, Y. R. Liu, C. H. Zhang, H. Zhang, Y. X. Liu, W. H. Pang, and Y. H. Zhang (2007), Zircon SHRIMP U–Pb dating of the tuff bed of Lengjiaxi and Banxi groups, northeastern Hunan: Constraints on the Wuling Movement [in Chinese with English abstract], *Geol. Bull. China*, *30*(7), 1001–1008.
- Gao, L. Z., M. G. Yang, X. Z. Ding, Y. X. Liu, X. Liu, L. H. Ling, and C. H. Zhang (2008), SHRIMP U–Pb zircon dating of tuff in the Shuangqiaoshan and Heshangzhen groups in South China: Constraints on the evolution of the Jiangnan Neoproterozoic orogenic belt, *Geol. Bull. China*, *27*, 1744–1758.
- Gao, L. Z., C. G. Dai, Y. X. Liu, M. Wang, X. H. Wang, J. S. Chen, X. Z. Ding, C. H. Zhang, X. Cao, and J. H. Liu (2010), Zircon SHRIMP U–Pb dating of tuff bed of the Sibao Group in southeastern Guizhou-northern Guangxi area, China and its stratigraphic implication, *Geol. Bull. China*, *29*, 1259–1267.
- Gao, L. Z., Z. Z. Huang, X. Z. Ding, Y. X. Liu, J. F. Pang, and C. H. Zhang (2012), Zircon SHRIMP U–Pb dating of Xiushui and Majianqiao Formations in northwestern Jiangxi Province [in Chinese with English abstract], *Geol. Bull. China*, *31*(7), 1086–1093.
- Gao, S., J. Yang, L. Zhou, M. Li, Z. C. Hu, J. L. Guo, H. L. Yuan, H. J. Gong, G. Q. Xiao, and J. Q. Wei (2011), Age and growth of the Archean Kongling terrain, South China, with emphasis on 3.3 Ga granitoid gneisses, *Am. J. Sci.*, *311*, 153–182.
- Gilder, S. A., G. R. Keller, M. Luo, and P. C. Goodell (1991), Timing and spatial distribution of rifting in China, *Tectonophysics*, *197*, 225–243.
- Gilder, S. A., J. Gill, R. S. Coe, X. X. Zhao, Z. W. Liu, G. X. Wang, K. R. Yuan, W. L. Liu, G. D. Kuang, and H. R. Wu (1996), Isotopic and paleomagnetic constraints on the Mesozoic tectonic evolution of South China, *J. Geophys. Res.*, *101*(7), 16,137–16,154, doi:10.1029/96JB00662.
- Goodge, J. W., V. L. Hansen, S. M. Peacock, B. K. Smith, and N. W. Walker (1993), *Tectonics*, *12*, 1460–1478, doi:10.1029/93TC02192.
- Grabau, A. (1924), *Stratigraphy of China, Part I, Paleozoic and Older*, Geol. Surv. of Agric. and Commerce, Peking.
- Guo, L. Z., Y. S. Shi, H. F. Lu, R. S. Ma, H. G. Dong, and S. F. Yang (1989), The pre-Devonian tectonic patterns and evolution of South China, *J. Southeast Asian Earth Sci.*, *3*, 87–93.
- Guo, L. Z., L. S. Shu, Y. S. Shi, H. F. Lu, R. S. Ma, Q. L. Zhang, and D. Jia (1996), Research on the terrane tectonics in China, *Chin. J. Geochem.*, *15*(3), 193–202.
- Hacker, B. R., L. Ratschbacher, L. Webb, T. Ireland, D. Walker, and S. W. Dong (1998), U–Pb zircon ages constrain the architecture of the ultrahigh-pressure Qinling-Dabie Orogen, China, *Earth Planet. Sci. Lett.*, *161*, 215–230.
- Halpin, J. A., H. T. Tran, C. K. Lai, S. Meffre, A. J. Crawford, and K. Zaw (2015), U–Pb zircon geochronology and geochemistry from NE Vietnam: A 'tectonically disputed' territory between the Indochina and South China blocks, *Gondwana Res.*, doi:10.1016/j.gr.2015.04.005.

- Han, Z. R., Z. Y. Yang, Y. B. Tong, and X. Q. Jing (2015), New paleomagnetic results from Late Ordovician rocks of the Yangtze Block, South China, and their paleogeographic implications, *J. Geophys. Res. Solid Earth*, *120*, 4759–4772, doi:10.1002/2015JB012005.
- HGBMR (Hunan Bureau of Geology and Mineral Resources) (1976), Regional geological map of the Liuyang area [in Chinese], in Hunan Province.
- Hippert, J., and E. Tohver (1999), On the development of zones of reverse shearing in mylonitic rocks, *J. Struct. Geol.*, *21*, 1603–1614.
- Holcombe, R. J., P. J. Pearson, and N. H. S. Oliver (1991), Geometry of a Middle Proterozoic extensional decollement in northeastern Australia, *Tectonophysics*, *191*, 255–274.
- Hsu, K. J., S. Sun, J. L. Li, and H. H. Chen (1990), Tectonics of South China: Key to understanding West Pacific geology, *Tectonophysics*, *183*, 9–39.
- Huang, J., J. Ren, C. Jiang, Z. Zhang, and D. Qin (1980), *The Tectonic Evolution of China*, pp. 124, Science Press, Beijing.
- Ichikawa, K., S. Mizutani, and I. Hara (1990), *Pre-Cretaceous Terranes of Japan*, pp. 413, Pre-Jurassic evolution of Eastern Asia, Osaka.
- Jahn, B. M., P. Y. Chen, and T. P. Yen (1976), Rb–Sr ages of granitic rocks in southeastern China and their tectonic significance, *Geol. Soc. Am. Bull.*, *87*(5), 763–776.
- JGBMR (Hunan Bureau of Geology and Mineral Resources) (1979), Regional geological map of the Tonggu area [in Chinese], in Jiangxi Province.
- Jiang, Y. H., P. Zhao, Q. Zhou, S. Y. Liao, and G. D. Jin (2011), Petrogenesis and tectonic implications of Early Cretaceous S- and A-type granites in the northwest of the Gan-Hang rift, SE China, *Lithos*, *121*, 55–73.
- Jordan, T. E., B. L. Isacks, R. W. Allmendinger, J. A. Brewer, V. A. Ramos, and C. J. Ando (1983), Andean tectonics related to geometry of subducted Nazca plate, *Geol. Soc. Am. Bull.*, *94*, 341–361.
- Kusky, T. M., M. Abdelsalam, R. J. Stern, and R. D. Tucker (2003), Evolution of the East African and related orogens, and the assembly of Gondwana, *Precambrian Res.*, *123*, 81–85.
- Kusky, T. M., M. H. Ye, J. P. Wang, and L. Wang (2010), Geological evolution of Longhushan World Geopark in relation to global tectonics, *J. Earth Sci.*, *21*(1), 1–18.
- Lepvrier, C., H. Maluski, V. V. Tich, A. Leyerloup, T. P. Truong, and V. V. Nguyen (2004), The Early Triassic Indosinian orogeny in Vietnam (Truong Son Belt and Kontum massif): Implications for the geodynamic evolution of Indochina, *Tectonophysics*, *393*, 87–118, doi:10.1016/j.tecto.2004.07.030.
- Li, H. K., S. X. Zhu, Z. Q. Xing, W. B. Su, S. N. Lu, H. Y. Zhou, J. Z. Geng, S. Li, and F. J. Yang (2010), Zircon U–Pb dating on tuff bed from Gaoyuzhuang Formation in Yanqing, Beijing: Further constraints on the new subdivision of the Mesoproterozoic stratigraphy in the northern North China Craton [in Chinese with English abstract], *Acta Petrol. Sin.*, *26*(7), 2131–2140.
- Li, J. H., Y. Q. Zhang, S. W. Dong, and H. L. Li (2012), Late Mesozoic–Early Cenozoic deformation history of the Yuanma Basin, central South China, *Tectonophysics*, *570–571*, 163–183.
- Li, J. H., Y. Q. Zhang, S. W. Dong, J. B. Su, Y. Li, J. J. Cui, and W. Shi (2013), The Hengshan low angle normal fault zone: Structural and geochronological constraints on the Late Mesozoic crustal extension in South China, *Tectonophysics*, *606*, 97–115.
- Li, J. H., Y. Q. Zhang, S. W. Dong, and S. T. Johnston (2014a), Cretaceous tectonic evolution of South China: A preliminary synthesis, *Earth Sci. Rev.*, *134*, 98–136.
- Li, J. H., Z. L. Ma, Y. Q. Zhang, S. W. Dong, Y. Li, M. A. Lu, and J. Q. Tan (2014b), Tectonic evolution of Cretaceous extensional basins in Zhejiang Province, eastern South China: Structural and geochronological constraints, *Int. Geol. Rev.*, *56*(13), 1602–1629.
- Li, J. H., W. Shi, Y. Q. Zhang, S. W. Dong, and Z. L. Ma (2015a), Thermal evolution of the Hengshan extensional dome in central South China and its tectonic implications: New insights into low-angle detachment formation, *Gondwana Res.*, doi:10.1016/j.gr.2015.06.008.
- Li, J. H., Y. Q. Zhang, S. W. Dong, Z. L. Ma, and Y. Li (2015b), LA-MC-ICPMS Zircon U–Pb geochronology of the Hongxiaqiao and Banshanpu granitoids in eastern Hunan Province and its geological implications, *Acta Geosci. Sin.*, *36*(2), 187–196.
- Li, J. H., S. W. Dong, A. Yin, Y. Q. Zhang, and W. Shi (2015c), Mesozoic tectonic evolution of the Daba Shan Thrust Belt in the southern Qinling orogen, central China: Constraints from surface geology and reflection seismology, *Tectonics*, *34*, 1545–1575, doi:10.1002/2014TC003813.
- Li, X. H. (1999), U–Pb zircon ages of granites from the southern margin of the Yangtze Block: Timing of Neoproterozoic Jinning Orogeny in SE China and implications for Rodinia assembly, *Precambrian Res.*, *97*, 43–57.
- Li, X. H. (2000), Cretaceous magmatism and lithosphere extension in southeast China, *J. Asian Earth Sci.*, *18*, 293–305.
- Li, X. H., G. Q. Zhou, J. X. Zhao, C. M. Fanning, and W. Compston (1994), SHRIMP ion microprobe zircon U–Pb age and Sm–Nd isotopic characteristics of the NE Jiangxi ophiolite and its tectonic implications, *Chin. J. Geochem.*, *13*, 317–325.
- Li, X. H., Z. X. Li, W. C. Ge, H. W. Zhou, W. X. Li, Y. Liu, and M. T. D. Wingate (2003), Neoproterozoic granitoids in South China: Crustal melting above a mantle plume at ca 825 Ma?, *Precambrian Res.*, *122*, 45–83.
- Li, X. H., W. X. Li, Z. X. Li, C. H. Lo, J. Wang, M. F. Ye, and Y. H. Yang (2009), Amalgamation between the Yangtze and Cathaysia Blocks in South China: Constraints from SHRIMP U–Pb zircon ages, geochemistry and Nd–Hf isotopes of the Shuangxiwu volcanic rocks, *Precambrian Res.*, *174*, 117–128.
- Li, X. H., Z. X. Li, B. He, W. X. Li, Q. L. Li, Y. Y. Gao, and X. C. Wang (2011), The Early Permian active continental margin and crustal growth of the Cathaysia Block: In situ U–Pb, Lu–Hf and O isotope analyses of detrital zircons, *Chem. Geol.*, doi:10.1016/j.chemgeo.2011.10.027.
- Li, Y., Y. Q. Zhang, J. B. Su, J. H. Li, and S. W. Dong (2015), Zircon U–Pb dating of Dayishan and Tashan Plutons in Hunan Province and its tectonic implications [in Chinese with English abstract], *Acta Geosci. Sin.*, *36*(3), 303–312.
- Li, Z. X. (1994), Collision between the North and South China blocks: A crustal-detachment model for suturing in the region east of the Tanlu fault, *Geology*, *22*, 739–742.
- Li, Z. X., and X. H. Li (2007), Formation of the 1300-km-wide intracontinental orogen and postorogenic magmatic province in Mesozoic South China: A flat-slab subduction model, *Geology*, *35*(2), 179–182.
- Li, Z. X., X. H. Li, P. Kinny, and J. Wang (1999), The breakup of Rodinia: Did it start with a mantle plume beneath South China, *Earth Planet. Sci. Lett.*, *173*, 171–181.
- Li, Z. X., X. H. Li, H. Zhou, and P. D. Kinny (2002), Grenvillian continental collision in South China: New SHRIMP U–Pb zircon results and implications for the configuration of Rodinia, *Geology*, *30*, 163–166.
- Li, Z. X., J. A. Wartho, S. Occhipinti, C. L. Zhang, X. H. Li, J. Wang, and C. M. Bao (2007), Early history of the eastern Sibao orogen (South China) during the assembly of Rodinia: New mica  $^{40}\text{Ar}/^{39}\text{Ar}$  dating and SHRIMP U–Pb detrital zircon provenance constraints, *Precambrian Res.*, *159*, 79–94.
- Li, Z. X., X. H. Li, J. A. Wartho, C. Clark, W. X. Li, C. L. Zhang, and C. Bao (2010), Magmatic and metamorphic events during the early Paleozoic Wuyi–Yunkai orogeny, south-eastern South China: New age constraints and pressure–temperature conditions, *Geol. Soc. Am. Bull.*, *122*, 772–793.
- Li, Z. X., X. H. Li, S. L. Chuag, C. H. Lo, X. S. Xu, and W. X. Li (2012), Magmatic switch-on and switch-off along the South China continental margin since the Permian: Transition from an Andean-type to a Western Pacific-type plate boundary, *Tectonophysics*, *532–535*, 271–290.
- Lin, S. F. (1995), Collision between the North and South China blocks: A crustal-detachment model for suturing in the region east of the Tanlu fault: Comment and Reply, *Geology*, *23*, 574–576.

- Lin, W., M. Faure, P. Monie, U. Schärer, L. Zhang, and Y. Sun (2000), Tectonics of SE China: New insights from the Lushan massif (Jiangxi Province), *Tectonics*, *19*, 852–871, doi:10.1029/2000TC900009.
- Lin, W., Q. C. Wang, and K. Chen (2008), Phanerozoic tectonic of South China block: New insights from the polyphase deformation in the Yunkai massif, *Tectonics*, *27*, TC6004, doi:10.1029/2007TC002207.
- Lister, G. S. (1977), Cross-girdle c-axis fabric in quartzites plastically deformed by plane strain and progressive simple shear, *Tectonophysics*, *1*, 51–54.
- Livaccari, R. F., K. Burke, and A. M. C. Sengor (1981), Was the Laramide orogeny related to subduction of an oceanic plateau?, *Nature*, *289*, 276–278.
- Ludwig, K. R. (2003), User's Manual for Isoplot 3.00. A Geochronological Toolkit for Microsoft Excel, Berkeley Geochronology Center, 70 p.
- Maruyama, S. (1997), Pacific-type orogeny revisited: Miyashiro-type orogeny proposed, *Island Arc*, *6*, 91–120.
- Meert, J. G. (2003), A synopsis of events related to the assembly of eastern Gondwana, *Tectonophysics*, *362*, 1–40.
- Mei, L. F., Z. Q. Liu, J. G. Tang, C. B. Shen, and Y. F. Fan (2010), Mesozoic intra-continental progressive deformation in the western Hunan–Hubei–Eastern Sichuan province of China: Evidence from apatite fission track and balanced cross-section [in Chinese with English abstract], *Earth Sci. J. China Univ. Geo sci.*, *35*(2), 161–174.
- Metcalfe, I. (2013), Gondwana dispersion and Asian accretion: Tectonic and palaeogeographic evolution of eastern Tethys, *J. Asian Earth Sci.*, *66*, 1–33.
- Minato, M., and M. Hunahashi (1985), Crustal Structure of the Japanese Islands, Japan Sea, Coastal Part of Western Pacific and Philippine Sea, *Bull. Japan Sea Res. Inst., Kanazawa Univ.*, *17*, 13–42.
- Murphy, J. B., A. J. Hynes, S. T. Johnston, and J. D. Keppie (2003), Reconstructing the ancestral Yellowstone plume from accreted seamounts and its relationship to flat-slab subduction, *Tectonophysics*, *365*, 185–194.
- Shi, W., S. W. Dong, Y. Q. Zhang, and S. Q. Huang (2015), The typical large-scale superposed folds in the central South China: Implications for Mesozoic intracontinental deformation of the South China Block, *Tectonophysics*, doi:10.1016/j.tecto.2015.08.039.
- Shu, L., and J. Charvet (1996), Kinematics and geochronology of the Proterozoic Dongxiang–Shexian ductile shear zone: With HP metamorphism and ophiolitic melange (Jiangnan Region, South China), *Tectonophysics*, *267*, 291–302.
- Shu, L. S. (2006), Predevonian tectonic evolution of South China: From Cathaysian Block to Caledonian Period folded orogenic belt [in Chinese with English abstract], *Geol. J. China Univ.*, *12*(4), 418–431.
- Shu, L. S. (2012), An analysis of principal features of tectonic evolution in South China block [in Chinese with English abstract], *Geol. Bull. China*, *31*(7), 1035–1053.
- Shu, L. S., J. Charvet, Y. S. Shi, M. Faure, D. Cluzel, and L. Z. Guo (1991), Structural analysis of the Nanchang–Wanzai sinistral ductile shear zone (Jiangnan region, South China), *J. Southeast Asian Earth Sci.*, *6*(1), 13–23.
- Shu, L. S., H. F. Lu, D. Jia, J. Charvet, and M. Faure (1999), Study of the  $^{40}\text{Ar}/^{39}\text{Ar}$  isotopic age for the early Paleozoic tectonothermal event in the Wuyishan region, South China [in Chinese with English abstract], *J. Nanjing Univ. (Nat. Sci.)*, *35*(6), 668–674.
- Shu, L. S., J. H. Yu, D. Jia, B. Wang, W. Z. Shen, and Y. Q. Zhang (2008a), Early Paleozoic orogenic belt in the eastern segment of South China [in Chinese with English abstract], *Geol. Bull. China*, *27*(10), 1081–1093.
- Shu, L. S., M. Faure, B. Wang, X. M. Zhou, and B. Song (2008b), Late Paleozoic–Early Mesozoic geological features of South China: Response to the Indosinian collision event in Southeast Asia, *C. R. Geosci.*, *340*(2–3), 151–165.
- Shu, L. S., X. M. Zhou, P. Deng, B. Wang, S. Y. Jiang, J. H. Yu, and X. X. Zhao (2009), Mesozoic tectonic evolution of the southeast China block: New insights from basin analysis, *J. Asian Earth Sci.*, *34*, 376–391.
- Shu, L. S., M. Faure, J. H. Yu, and B. M. Jahn (2011), Geochronological and geochemical features of the Cathaysia Block (South China): New evidence for the Neoproterozoic breakup of Rodinia, *Precambrian Res.*, *187*, 263–276.
- Shu, L. S., B. M. Jahn, J. Charvet, M. Santosh, B. Wang, X. S. Xu, and S. Y. Jiang (2014), Intraplate tectono-magmatism in the Cathaysia Block (South China): Evidence from stratigraphic, structural, geochemical and geochronological investigations, *Am. J. Sci.*, *314*, 154–186.
- Shu, L. S., B. Wang, P. A. Cawood, M. Santosh, and Z. Q. Xu (2015), Early Paleozoic and Early Mesozoic intraplate tectonic and magmatic events in the Cathaysia Block, South China, *Tectonics*, *34*, 1600–1621, doi:10.1002/2015TC003835.
- Shu, L., G. Zhou, Y. Shi, and J. Yin (1994), A study on the high pressure metamorphic blueschist and its late Proterozoic age in the Eastern Jiangnan belt, *Chin. Sci. Bull.*, *39*, 1200–1204.
- Song, M. J., L. S. Shu, M. Santosh, and Y. Y. Li (2015), Late Early Paleozoic and Early Mesozoic intracontinental orogeny in the South China Craton: Geochronological and geochemical evidence, *Lithos*, *232*, 360–374.
- Stipp, M., H. Stünitz, R. Heilbronner, and S. M. Schmid (2002), The eastern Tonale fault zone: A “natural laboratory” for crystal plastic deformation of quartz over a temperature range from 250 to 700°C, *J. Struct. Geol.*, *24*, 1861–1884.
- Sylvester, A. G. (1988), Strike-slip faults, *Geol. Soc. Am. Bull.*, *100*, 1666–1703.
- Ting, W. K. (1929), The orogenic movement in China, *Bull. Geol. Soc. China*, *8*(1), 151–170.
- Wang, D. Z., and L. S. Shu (2012), Late Mesozoic basin and range tectonics and related igneous rock assemblages of Southeast China, *Geosci. Front.*, *3*(2), 109–124.
- Wang, J., and Z. X. Li (2003), History of Neoproterozoic rift basins in South China: Implications for Rodinia break-up, *Precambrian Res.*, *122*(1–4), 141–158.
- Wang, J. G., S. Q. Yu, Y. H. Hu, X. D. Zhao, M. Wu, and M. G. Gu (2014), The discovery, petrology and geochronology of the retrograde eclogite in Jiangshan–Shaoxing suture zone [in Chinese with English abstract], *Geol. China*, *41*(4), 1356–1363.
- Wang, J. Q., L. S. Shu, and J. H. Yu (2016), Petrological properties and tectonic significance for Longyou garnet amphibolite [in Chinese with English abstract], *Chin. Sci. Bull.*, *61*, 125–134.
- Wang, X. L., J. C. Zhou, W. L. Griffin, R. C. Wang, J. S. Qiu, S. Y. O'Reilly, X. S. Xu, X. M. Liu, and G. L. Zhang (2007), Detrital zircon geochronology of Precambrian basement sequences in the Jiangnan orogen: Dating the assembly of the Yangtze and Cathaysia blocks, *Precambrian Res.*, *159*, 117–131.
- Wang, X. W., Y. J. Wo, and R. Q. Zhang (2008), Tectonic–sedimentary cycle of the Yangtze Craton from Nanhua to the Early Paleozoic [in Chinese with English abstract], *Geoscience*, *22*(4), 525–533.
- Wang, Y. J., Y. H. Zhang, W. M. Fan, and T. P. Peng (2005), Structural signatures and  $^{40}\text{Ar}/^{39}\text{Ar}$  geochronology of the Indosinian Xuefengshan transpressive belt, south China interior, *J. Struct. Geol.*, *27*, 985–998.
- Wang, Y. J., W. M. Fan, G. C. Zhao, S. C. Ji, and T. P. Peng (2007), Zircon U–Pb geochronology of gneisses in Yunkai Mountains and its implications on the Caledonian event in South China, *Gondwana Res.*, *12*(4), 404–416.
- Wang, Y. J., F. F. Zhang, W. M. Fan, G. W. Zhang, S. Y. Chen, P. A. Cawood, and A. M. Zhang (2010), Tectonic setting of the South China block in the Early Paleozoic: Resolving intracontinental and ocean closure models from detrital zircon U–Pb geochronology, *Tectonics*, *29*, TC6020, doi:10.1029/2010TC002750.

- Wang, Y. J., A. M. Zhang, W. M. Fan, G. C. Zhao, G. W. Zhang, F. F. Zhang, Y. Z. Zhang, and S. Z. Li (2011), Kwangian crustal anatexis within the eastern South China Block: Geochemical, zircon U-Pb geochronological and Hf isotopic fingerprints from the gneissoid granites of Wugong and Wuyi-Yunkai Domains, *Lithos*, *127*, 239–260.
- Wang, Y. J., C. M. Wu, A. M. Zhang, W. M. Fan, Y. H. Zhang, Y. Z. Zhang, T. P. Peng, and C. Q. Yin (2012), Kwangian and Indosinian reworking of the eastern South China Block: Constraints on zircon U-Pb geochronology and metamorphism of amphibolite and granulite, *Lithos*, doi:10.1016/j.lithos.2012.04.022.
- Wang, Y. J., W. M. Fan, G. W. Zhang, and Y. H. Zhang (2013a), Phanerozoic tectonics of the South China Block: Key observations and controversies, *Gondwana Res.*, *23*, 1273–1305.
- Wang, Y. J., A. M. Zhang, P. Q. Cawood, W. M. Fan, J. F. Xu, G. W. Zhang, and Y. Z. Zhang (2013b), Geochronological, geochemical and Nd-Hf-Os isotopic fingerprinting of an early Neoproterozoic arc-back-arc system in South China and its accretionary assembly along the margin of Rodinia, *Precambrian Res.*, *231*, 343–371.
- Wang, Y., W. Fan, P. A. Cawood, S. Ji, T. Peng, and X. Chen (2007c), Indosinian high-strain deformation for the Yunkaidashan tectonic belt, south China: Kinematics and  $^{40}\text{Ar}/^{39}\text{Ar}$  geochronological constraints, *Tectonics*, *26*, TC6008, doi:10.1029/2007TC002099.
- Xu, B., L. Z. Guo, and Y. S. Shi (1992), *Proterozoic Terranes and Multiphase Collision Orogenesis Anhui-Zhejiang-Jiangxi Area* [in Chinese with English abstract], pp. 1–112, Geological Publishing House, Beijing.
- Xu, D., B. Xia, N. Bakun-Czubarow, R. Bachlinski, P. Li, G. Chen, and T. Chen (2008), Geochemistry and Sr-Nd isotope systematics of metabasites in the Tunchang area, Hainan Island, South China: Implications for petrogenesis and tectonic setting, *Mineral. Petrol.*, *92*, 361–391.
- Xu, D. R., B. Xia, P. C. Li, G. H. Chen, C. Ma, and Y. Q. Zhang (2007), Protolith natures and U-Pb sensitive high mass-resolution ion microprobe (SHRIMP) zircon ages of the metabasites in Hainan Island, South China: Implications for geodynamic evolution since the late Precambrian, *Island Arc*, *16*, 575–597.
- Xu, X. B., Y. Q. Zhang, D. Jia, and L. S. Shu (2009), Early Mesozoic geotectonic processes in South China [in Chinese with English abstract], *Geol. China*, *36*(3), 573–593.
- Xu, X. B., Y. Q. Zhang, L. S. Shu, and D. Jia (2011), La-ICP-MS U-Pb and  $^{40}\text{Ar}/^{39}\text{Ar}$  geochronology of the sheared metamorphic rocks in the Wuyishan: Constraints on the timing of Early Paleozoic and Early Mesozoic tectono-thermal events in SE China, *Tectonophysics*, *501*(1–4), 71–86.
- Xu, X. B., Y. Li, S. Tang, D. J. Xue, and Z. J. Zhang (2015), Neoproterozoic to Early Paleozoic polyorogenic deformation in the southeastern margin of the Yangtze Block: Constraints from structural analysis and  $^{40}\text{Ar}/^{39}\text{Ar}$  geochronology, *J. Asian Earth Sci.*, *98*, 141–151.
- Xu, Y. J., P. A. Cawood, Y. S. Du, H. W. Huang, and X. Y. Wang (2014a), Early Paleozoic orogenesis along Gondwana's northern margin constrained by provenance data from South China, *Tectonophysics*, *636*, 40–51, doi:10.1016/j.tecto.2014.08.022.
- Xu, Y. J., P. A. Cawood, Y. S. Du, Z. Q. Zhong, and N. C. Hughes (2014b), Terminal suturing of Gondwana along the southern margin of South China Craton: Evidence from detrital zircon U-Pb ages and Hf isotopes in Cambrian and Ordovician strata, Hainan Island, *Tectonics*, *33*, 2490–2504, doi:10.1002/2014TC003748.
- Yan, D. P., M. F. Zhou, H. L. Song, X. W. Wang, and J. Malpas (2003), Origin and tectonic significance of a Mesozoic multi-layer over-thrust system within the Yangtze block (South China), *Tectonophysics*, *361*, 239–254.
- Yan, D. P., B. Zhang, M. F. Zhou, G. Q. Wei, H. L. Song, and S. F. Liu (2009), Constraints on the depth, geometry and kinematics of blind detachment faults provided by fault-propagation folds: An example from the Mesozoic fold belt of South China, *J. Struct. Geol.*, *31*, 150–162.
- Yang, M. G., J. G. Wang, Y. Li, Z. B. Yao, X. J. Wei, J. H. Li, and J. H. Zhang (1994), Regional geology of South China, in *Outline of Regional Geology of China* [in Chinese], edited by Y. Q. Cheng, pp. 313–384, Geological Publishing House, Beijing.
- Yang, S. X., and P. R. Yu (1994), The characteristics of shallower imbricate nappe structure along Pushi-Chenxi and its significance in searching mineral resources [in Chinese with English abstract], *Hunan Geol.*, *14*(1), 31–34.
- Yang, Z. Y., Z. M. Sun, T. S. Yang, and J. L. Pei (2004), A long connection (750–380 Ma) between South China and Australia: Paleomagnetic constraints, *Earth Planet. Sci. Lett.*, *220*(3–4), 423–434.
- Yao, J. L., L. S. Shu, M. Santosh, and G. C. Zhao (2014), Neoproterozoic arc-related mafic-ultramafic rocks and syn-collision granite from the western segment of the Jiangnan Orogen, South China: Constraints on the Neoproterozoic assembly of the Yangtze and Cathaysia Blocks, *Precambrian Res.*, *243*, 39–62.
- Yao, J. L., L. S. Shu, M. Santosh, and J. Y. Li (2015), Neoproterozoic arc-related andesite and orogeny-related unconformity in the eastern Jiangnan orogenic belt: Constraints on the assembly of the Yangtze and Cathaysia blocks in South China, *Precambrian Res.*, *262*, 84–100.
- Yi, L. W., C. Q. Ma, L. X. Wang, Z. X. Lai, X. Y. Li, Y. N. Yang, F. Wu, and Y. R. Hu (2014), Discovery of late Ordovician subvolcanic rocks in South China: Existence of subduction-related dacite from early Paleozoic [in Chinese with English abstract], *Earth Sci.-J. China Univ. Geosci.*, *39*(6), 637–653.
- Yin, A., and S. Nie (1993), An indentation model for the north and south China collision and the development of the Tan-Lu and Honam fault systems, eastern Asia, *Tectonics*, *12*, 801–813, doi:10.1029/93TC00313.
- Yin, A., and S. Y. Nie (1996), A Phanerozoic reconstruction of China and its neighboring regions, in *The Tectonics of Asia*, edited by A. Yin and T. M. Harrison, pp. 442–485, Cambridge Univ. Press, New York.
- Yin, C. Q. (2014), Is the South China Block an accretionary orogeny? Insights from recent geological and geochronological data and lessons from the Appalachian-Caledonian Orogeny, GSA Annual Meeting in Vancouver, British Columbia.
- Yin, C. Q., S. F. Lin, D. W. Davis, G. F. Xing, W. J. Davis, G. H. Cheng, W. J. Xiao, and L. M. Li (2013), Tectonic evolution of the southeastern margin of the Yangtze Block: Constraints from SHRIMP U-Pb and LA-ICP-MS Hf isotopic studies of zircon from the eastern Jiangnan Orogenic Belt and implications for the tectonic interpretation of South China, *Precambrian Res.*, *236*, 145–156.
- Yuan, Y., Z. T. Liao, and C. Wang (2012), Multi-stage tectonic evolution in Jiangnan uplift (Jiuling terrane) from granitoids records [in Chinese with English abstract], *J. Tongji Univ. (Nat. Sci.)*, *40*(9), 1414–1421.
- Zhang, G. W., B. R. Zhang, X. C. Yuan, and Q. H. Xiao (2001), *Qinling Orogenic Belt and Continental Dynamics* [in Chinese with English abstract], pp. 1–855, Science Press, Beijing.
- Zhang, G. W., A. L. Guo, Y. J. Wang, S. Z. Li, Y. P. Dong, S. F. Liu, D. F. He, S. Y. Cheng, R. K. Lu, and A. P. Yao (2013), Tectonics of South China continent and its implications, *Sci. China Earth Sci.*, *56*(11), 1804–1828.
- Zhang, K. J., and J. X. Cai (2009), NE-SW-trending Hepu-Hetai dextral shear zone in southern China: Penetration of the Yunkai promontory of South China into Indochina, *J. Struct. Geol.*, *31*, 737–748.
- Zhang, R., et al. (1990), *Precambrian Geology of Hainan Island, South China* [in Chinese with English abstract], Wuhan, China Univ. Geosci. Press.
- Zhang, S. B., R. X. Wu, and Y. F. Zheng (2012), Neoproterozoic continental accretion in South China: Geochemical evidence from the Fuchuan ophiolite in the Jiangnan orogen, *Precambrian Res.*, *220–221*, 45–64.
- Zhang, Y. J., X. H. Zhou, S. B. Liao, X. D. Zhang, B. Wu, C. Z. Wang, and M. G. Yu (2010), Neoproterozoic crustal composition and orogenic process of the Zhanggongshan area, Anhui-Jiangxi [in Chinese with English abstract], *Acta Geol. Sin.*, *84*(10), 1401–1427.

- Zhang, Y. Q., X. B. Xu, D. Jia, and L. S. Shu (2008), Deformation record of the change from Indosinian collision-related tectonic system to Yanshanian subduction-related tectonic system in South China during the Early Mesozoic [in Chinese with English abstract], *Earth Sci. Front.*, *15*(6), 1–14.
- Zhang, Y. Z., Y. J. Wang, H. Y. Geng, Y. H. Zhang, W. M. Fan, and H. Zhong (2013), Early Neoproterozoic (~850 Ma) back-arc basin in the Central Jiangnan Orogen (Eastern South China): Geochronological and petrogenetic constraints from meta-basalts, *Precambrian Res.*, *231*, 325–342.
- Zhao, G. C. (2015), Jiangnan Orogen in South China: Developing from divergent double subduction, *Gondwana Res.*, *27*, 1173–1180.
- Zhao, G. C., and P. A. Cawood (1999), Tectonothermal evolution of the Mayuan assemblage in the Cathaysia Block: New evidence for Neoproterozoic collisional-related assembly of the South China Craton, *Am. J. Sci.*, *299*, 309–339.
- Zhao, G. C., and P. A. Cawood (2012), Precambrian geology of China, *Precambrian Res.*, *222–223*, 13–54.
- Zhao, X. X., and R. Coe (1987), Palaeomagnetic constraints on the collision and rotation of north and south China, *Nature*, *327*, 141–144.
- Zheng, Y. F., R. X. Wu, Y. B. Wu, S. B. Zhang, H. L. Yuan, and F. Y. Wu (2008), Rift melting of juvenile arc-derived crust: Geochemical evidence from Neoproterozoic volcanic and granitic rocks in the Jiangnan Orogen, South China, *Precambrian Res.*, *163*, 351–383.
- Zhong, Y. F., C. Q. Ma, Z. B. Yu, G. C. Lin, H. J. Xu, R. J. Wang, K. G. Yang, and Q. Liu (2005), SHRIMP U–Pb zircon geochronology of the Jiuling granitic complex batholith in Jiangxi Province [in Chinese with English abstract], *Earth Sci. -J. China Univ. Geosci.*, *30*(6), 685–691.
- Zhong, Y. F., C. Q. Ma, Z. B. She, H. B. Xu, S. M. Wang, and L. X. Wang (2011), Geochemistry and genesis of Mengshan granitoids in north-western Jiangxi Province [in Chinese with English abstract], *Earth Sci. -J. China Univ. Geosci.*, *36*(4), 703–720.
- Zhou, J. C., S. Y. Jiang, X. L. Wang, J. H. Yang, and M. Q. Zhang (2005), Re–Os isochron age of Fankeng basalts from Fujian of SE China and its geological significance, *Geochem. J.*, *39*, 497–502.
- Zhou, M. F., D. P. Yan, A. K. Kennedy, Y. Li, and J. Ding (2002), SHRIMP U–Pb zircon geochronological and geochemical evidence for Neoproterozoic arc-magmatism along the western margin of the Yangtze Block, South China, *Earth Planet. Sci. Lett.*, *196*, 51–67.
- Zhou, X. M., and W. X. Li (2000), Origin of Late Mesozoic igneous rocks in southeastern China: Implications for lithosphere subduction and underplating of mafic magmas, *Tectonophysics*, *326*, 269–287.
- Zhou, X. M., H. B. Zou, J. D. Yang, and Y. X. Wang (1989), Sm–Nd isochron age of the Fuchuan Ophiolite Suite in Shexian, Anhui Province and its geological significance [in Chinese with English abstract], *Chin. Sci. Bull.*, *16*, 1243–1245.
- Zhou, X. M., T. Sun, W. Z. Shen, L. S. Shu, and Y. L. Niu (2006), Petrogenesis of Mesozoic granitoids and volcanic rocks in South China: A response to tectonic evolution, *Episodes*, *29*, 26–33.